https://doi.org/10.5194/essd-2022-195
Preprint. Discussion started: 3 August 2022

Open Access Earth System Science Data Discussions

A monthly 0.01° terrestrial evapotranspiration product (1982-2018) for the Tibetan Plateau

Ling Yuan [1, 2], Xuelong Chen[1,4*], Yaoming Ma[1, 2, 3, 4, 5, 6*], Cunbo Han[1,4], Binbin Wang[1,4], Weiqiang Ma[1,4]

[1] Land-Atmosphere Interaction and its Climatic Effects Group, State Key Laboratory of Tibetan Plateau Earth System, Resources and Environment (TPESRE), Institute of Tibetan Plateau Research, Chinese Academy of Sciences, Beijing 100101, China.

[2] College of Earth and Planetary Sciences, University of Chinese Academy of Sciences, Beijing 100049, China

[3] College of Atmospheric Science, Lanzhou University, Lanzhou 730000, China

[4] National Observation and Research Station for Qomolongma Special Atmospheric Processes and Environmental Changes, Dingri 858200, China

[5] Kathmandu Center of Research and Education, Chinese Academy of Sciences, Beijing 100101, China

[6] China-Pakistan Joint Research Center on Earth Sciences, Chinese Academy of Sciences, Islamabad 45320, Pakistan

Corresponding author and address:

Xuelong Chen, Dr., Prof., x.chen@itpcas.ac.cn

Yaoming Ma, Dr., Prof., ymma@itpcas.ac.cn

Building 3, No.16 Lincui Road, Chaoyang District, Beijing 100101, China

https://doi.org/10.5194/essd-2022-195
Preprint. Discussion started: 3 August 2022

Earth System Science Data
Open Access
Discussions

Abstract

Evapotranspiration (ET) is an important component of the water balance system in the "Asian water tower" region, the Tibetan Plateau (TP). However, accurately monitoring and understanding the spatial and temporal variability of the ET components (soil evaporation E_s, canopy transpiration $E_{c,}$ and intercepted water evaporation E_w) on the TP remains gravely challenging due to the paucity of observational data for this remote area. In this study, the 37 years (1982–2018) of monthly ET component data for the TP were produced using the MOD16-STM model, which uses the recently available soil properties, meteorological conditions, and remote sensing datasets. The estimated ET results correlate very well with the measurements from nine flux towers, with a low root mean square error of 13.48 mm/month, mean bias of 2.85 mm/month, coefficient of determination of 0.83, and index of agreement of 0.92. The annual average ET for the entire TP (specified as elevations higher than 2500 m) is about 0.93 ± 0.037 Gt/year. The main contribution of the ET on the TP comes from the soil, with the E_s accounting for more than 84% of the ET. During the study period, the ET exhibited a significant increasing trend, with rates of about 1–4 mm/year ($p < 0.05$), over most parts of the central and eastern TP and a significant decreasing trend, with rates of −3 to −1 mm/year, over the northwestern TP. The rate of increase in the ET on the TP over the past 37 years was around 0.96 mm/year. The increase in the ET over the entire TP from 1982 to 2018 can be explained by the warming and wetting trend of the climate on the TP during this period. The MOD16-STM ET data exhibited an acceptable performance over the TP compared with previous results. MOD16-STM ET can accurately estimate actual ET for research in water resource management, drought monitoring and ecological change. The whole datasets are freely available at the Science Data Bank (http://doi.org/10.11922/sciencedb.00020, Y. Ma*, X.Chen*, L. Yuan, 2021) and the National Tibetan Plateau Data Center (TPDC) (http://doi.org/10.11888/Terre.tpdc.271913, L. Yuan, X.Chen*, Y. Ma*, 2021).

Keywords: Long term variation of Evapotranspiration; MOD16-STM; Climate factors; Asian water tower; Tibetan Plateau

https://doi.org/10.5194/essd-2022-195
Preprint. Discussion started: 3 August 2022

1. Introduction

The Tibetan Plateau (TP) (24–40°N, 70–105°E) is known as the Asian water tower (Immerzeel et al., 2020; Yao et al., 2012; Xu et al., 2019) due to its unique geographical and ecological characteristics. Evapotranspiration (ET) is a very important component of the water balance of the Asian water tower. The land cover on the TP is predominantly grassland and sparse vegetation or bare soil (with coverages of >47% and >33%, respectively) based on the Moderate Resolution Imaging Spectroradiometer (MODIS) landcover (MCD12C1) dataset (Fig. 1c). Most of the TP is arid or semi-arid. The TP is experiencing accelerated changes in its hydrological cycle due to global warming (Yang et al., 2014; Kuang et al., 2016; Zohaib et al., 2017). Meanwhile, accurate monitoring of the spatial and temporal variability of the ET remains challenging due to the remote nature of the TP. In addition, how the ET over the TP will change under the background of global warming is critical for analyzing the impacts of changes in the water balance of the Asian water tower on the local people's lives.

In the last few years, a wide variety of ET datasets have been compiled to improve estimations of the ET on the TP, i.e., the complementary relationship (CR) model (Ma et al., 2019; Wang et al., 2020), the surface energy balance system (SEBS) model (Chen et al., 2014, 2021; Zhong et al., 2019; Han et al., 2017, 2021), and the Penman–Monteith model with remote sensing (RS-PM) (Wang et al., 2018; Song et al., 2017; Chang et al., 2019; Ma et al., 2022). Others have used reanalysis datasets (Shi et al., 2014; Dan et al., 2017; Yang et al., 2019; De Kok et al., 2020), pan observations (Xie et al., 2015; Zhang et al., 2018; Yao et al., 2019), and eddy-covariance (EC) (Shi et al., 2014; You et al., 2017; Yang et al., 2019; Ma et al., 2020) to study the ET on the TP. However, there is still a lack of longer-term remote sensing ET products for the TP, and there is considerable variance among the ET products for the TP (Peng et al., 2016; Baik et al., 2018; Li et al., 2018; Khan et al., 2018). Most of these ET products perform poorly in areas with sparse vegetation or arid to semi-arid climates, as well as in areas with inadequate water supplies. This is mainly due to the poor judgment of the ET dominant factors and the accuracy of the ET driving data used (Zhang et al., 2010; Li et al., 2014b; Song et al., 2017; Baik et al., 2018; Li et al., 2018; Khan et al., 2018). The MOD16 algorithm also separately estimates the canopy transpiration (E_c), soil evaporation (E_s), and interception (E_i) (Mu et al., 2011; Zhang et al., 2010), and it has been used for global ET estimations. However, the MOD16 ET product has some problems on the TP. The poor performance of the MOD16 model in the arid to semi-arid areas of the TP is due to the fact that the algorithm does not take into account the dominant role of the topsoil information (topsoil texture and topsoil moisture (SM)) in controlling the evaporation processes (Yuan et al., 2021). Although previous studies have obtained accurate ET estimates after improving the canopy conduction algorithm in the MOD16 model (Leuning et al., 2008; Zhang et al., 2010; Li et al., 2015; Zhang et al., 2016, 2019; Gan et al., 2018), it is also difficult to separate and

https://doi.org/10.5194/essd-2022-195
Preprint. Discussion started: 3 August 2022

validate the ET components effectively. Interestingly, there are significant differences in the global and regional contributions of the E_s, E_c, and E_i even if the total ET estimates are consistent across different products (Lawrence et al., 2007; Blyth and Harding, 2011; Miralles et al., 2016). The MOD16 model (MOD16-STM) was enhanced by redefining the E_s and E_c module with the help of EC observations from several flux sites on the TP (Yuan et al., 2021). The MOD16-STM model was validated at more independent stations (Appendix B). The Penman–Monteith–Leuning (PML) algorithm was used to test the good performance of the ET estimation on the TP (Wang et al., 2018; Ma et al., 2022). However, the effects of the SM on the evaporation resistance and stomatal conductance are not included in this model. Furthermore, the recent ET dataset (Han et al., 2021) based on the energy balance method does not cover a long enough time period for climate trend analysis (about 18 years, 2001–2018), and it does not estimate the ET components.

Es may account for the vast majority of ET in sparsely vegetated areas, especially in arid and semi-arid areas where bare soil areas are relatively large (Wilcox et al., 2003; Kool et al.,2014; Wang et al., 2018; Ma et al., 2022). Previous studies have pointed out that 20% to 40% of the global ET comes from Es (Lawrence et al., 2007; Schlesinger and Jasechko, 2014), which is a fast process influenced by shallow surface water (Koster and Suarez, 1996) and mainly controlled by soil vapor diffusion (Good et al., 2015; Yuan et al., 2022). Therefore, accurate quantification and separation of the E_s could help improve our understanding of the water and energy cycles on the TP. Nevertheless, quantifying the ET and its components remains a difficult task since it is controlled by the atmospheric demand, soil moisture conditions, and complex interactions between typical inhomogeneous vegetation and soil properties (Merlin et al., 2016; Wu et al., 2017; Philips et al., 2017; Lehmann et al., 2018). In this study, the MOD16-STM model, with its drawbacks fully in mind, was used to estimate a more accurate long-term ET (and its components) dataset (Yuan et al., 2021).

Currently, there are still no long-term variations in the ET estimation across the TP that incorporate soil information. Hence, based on the advantage of the MOD16-STM model for estimating ET on the TP, the goals of this study were (1) to develop a 37-year (1982–2018) 0.01 × 0.01 monthly ET dataset for the TP; and (2) to quantify the spatial distributions and spatiotemporal variability of the ET and its components over the TP.

2. Materials and methods

2.1 Study area

The Tibetan Plateau (25-40°N, 74-104°E) is about 2.5 million km^2 of land above 2,500 meters in altitudes) (Fig. 1a). It is the largest landform unit in Eurasia and mainly includes hyper-arid, arid, semi-arid, and sub-humid climate zones (Fig. 1b). The land cover types are mainly divided into mixed forest, grassland, bare soil, and glaciers and snow

https://doi.org/10.5194/essd-2022-195
Preprint. Discussion started: 3 August 2022

Open Access Earth System Science Data Discussions

(Fig. 1c). The topsoil is mainly covered with sandy loam, loam, and clay (Fig. 1d). The annual average temperature is about −3.1°C to 4.4°C. The average annual precipitation gradually increases from less than 50 mm in the northwest to more than 1000 mm in the southeast, and most of the precipitation is concentrated in the summer (Ding et al., 2017). The TP has experienced a significant warming trend over past decades (Chen et al., 2015), leading to significant changes in its environment, including increased precipitation; decreased wind speed, snow days, and radiation; and the thawing of permafrost, melting of glaciers, and greening of vegetation (Kang et al., 2010; Yao et al., 2012; Yang et al., 2014; Kuang et al., 2016; Bibi et al., 2018).

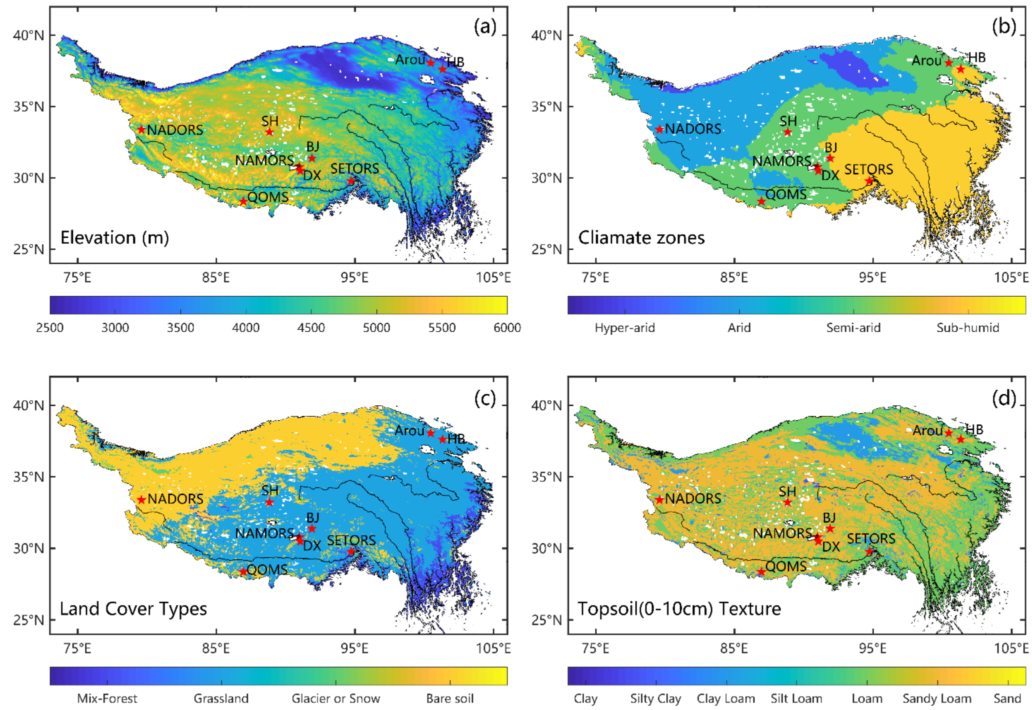

Figure 1 Maps of the (a) topography, (b) climate zones, (c) land cover types, and (d) soil textures in the study area. The red dots indicate the flux site locations.

2.2 How to generate a long-term series of monthly ET products？

2.2.1 Description of generating MOD16-STM ET in detail

In this study, a newly generated set of long-term series of monthly ET products is estimated based on the MOD16-STM model. The performance of the model is verified by the ET measurements at the flux station (Appendix A). The workflow for calculating the monthly ET using the MOD16-STM model and driving datasets is presented in Fig. 2.

https://doi.org/10.5194/essd-2022-195
Preprint. Discussion started: 3 August 2022

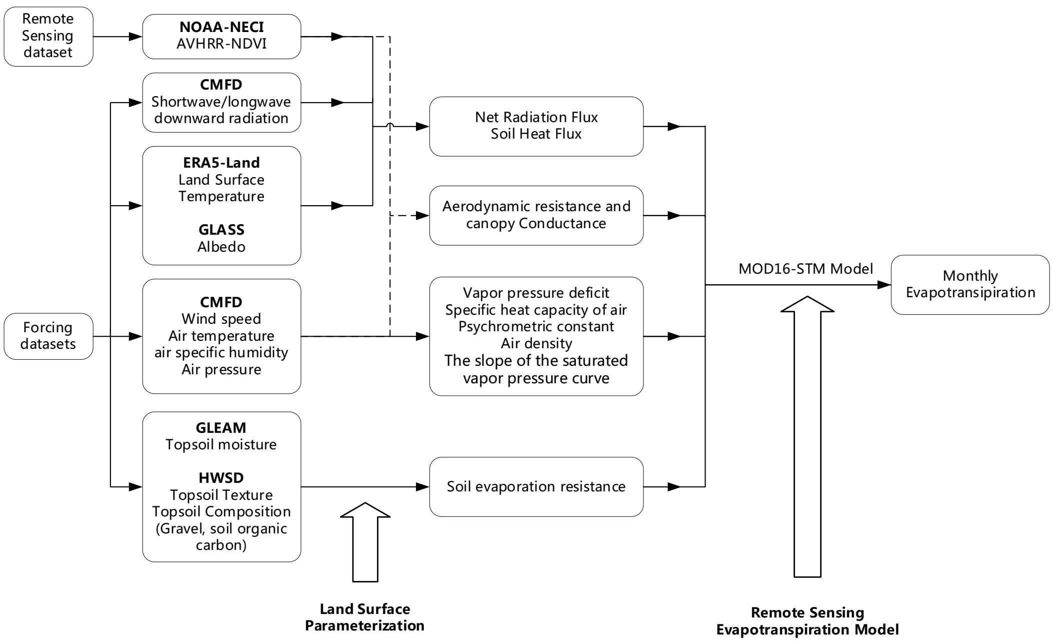

Figure 2 Workflow of the MOD16-STM evapotranspiration product.

The MOD16-STM model calculates the ET (or components) based on the Penman–Monteith equation as follows:

$$E_c = \frac{(\Delta \times f_c \times (R_n - G_0) + \rho_a \times C_p \times \frac{VPD}{r_a} \times f_c) \times (1 - F_{wet})}{\lambda \times \left(\Delta + \gamma \times (1 + \frac{r_s}{r_a}) \right)} \tag{1}$$

$$E_s = \frac{(\Delta \times (1 - f_c) \times (R_n - G_0) + \rho_a \times C_p \times \frac{VPD}{r_a}) \times (1 - F_{wet})}{\lambda \times \left(\Delta + \gamma \times (1 + \frac{r_s}{r_a}) \right)} \times \left(\frac{RH}{100} \right)^{\frac{VPD}{\beta}} \tag{2}$$

$$E_i = \frac{(\Delta \times (R_n - G_0) + \rho_a \times C_p \times \frac{VPD}{r_a}) \times F_{wet}}{\lambda \times \left(\Delta + \gamma \times (1 + \frac{r_s}{r_a}) \right)} \tag{3}$$

The ET is the sum of the components. Where R_n is the net radiation flux (W/m^2); G_0 is the soil heat flux (W/m^2); ρ_a
140 is the density of the air (kg/m^3); C_p is the specific heat capacity of the air (J/kg/K); VPD is the vapor pressure deficit (hPa); and Δ is the slope of the saturated vapor pressure curve (hPa/K). γ is the psychrometric constant (hPa/K), and $\gamma = C_p \cdot P_a \cdot M_a / (\lambda \cdot M_w)$, where λ is the latent heat of vaporization(J/kg), and M_a and M_w are the molecular masses of dry air and wet air, respectively. r_a is the aerodynamic resistance (s/m); and r_s is the surface (or canopy) resistance (s/m). the vegetation cover fraction (f_c) is estimated from the NDVI; and F_{wet} is the relative surface wetness. R_n and G_0 are

https://doi.org/10.5194/essd-2022-195
Preprint. Discussion started: 3 August 2022

calculated as follows:

$$R_n = (1-\alpha)\times SWD + LWD - \varepsilon\times\sigma\times LST^4 \tag{4}$$

$$G_0 = R_n \times (I_c + (1-f_c)\times(I_c - I_s)) \tag{5}$$

where σ is the Stefan-Boltzmann constant (5.67×10^{-8} W/m^2/K^4). I_c (=0.05) and I_s (=0.315) are the ratios of the full vegetation cover (Su et al., 2002) and ground heat flux and net radiation for surfaces with bare soil (differentiated by $NDVI < 0.25$ in this study) (Yuan et al., 2021), respectively. When $T_a < 5$°C, photosynthesis and transpiration are not active, so E_c is not taken into account. When the LST or $T_a < 0$°C, the sublimation equation is obtained by rewriting the surface energy balance equation using the Clausius–Clapeyron equation for (liquid and frozen) water-vapor equilibrium. The following form of the P-M combination equation was used:

$$ET = \frac{\Delta(R_n - G_0) + \rho_a C_p \dfrac{VPD}{r_a}}{\lambda(1+\gamma)} \tag{6}$$

Furthermore, the evaporation of surface water was not estimated in this study because previous studies have specifically studied the evaporation from the lakes on the TP in detail (Wang et al., 2020).

Many previous studies have used the optimized surface conductance to estimate the E_c (Jarvis et al., 1976; Irmak and Mutiibwa, 2010; Zhang et al., 2010; Leuning et al., 2008; Li et al., 2013, 2015), and the surface model and the PM equation to estimate the E_s (Sun et al., 1982; Camillo and Gurney, 1986; Sellers et al., 1996; Sakaguchi and Zeng, 2009; Ortega-Farias et al., 2010; Tang et al., 2013). In this study, the aerodynamic resistance (r_a) was calculated from the Monin-Obukhov similarity theory (MOST) (Thom, 1975), the roughness height of the momentum transfer (z_{0m}) was derived from the canopy height (h_c) following Chen et al. (2013), and the roughness heights of the water vapor transfer z_{0h} were derived as follows Yang et al. (2008):

$$r_a = \frac{\ln\left(\dfrac{z_h}{z_{0h}} - \psi_h\right)\ln\left(\dfrac{z_m}{z_{0m}} - \psi_m\right)}{k^2 u} \tag{7}$$

where k is the von Karman's constant (0.41), and z_h and z_m are the measurement heights of the T_a. ψ_m and ψ_h are the stability correction functions for the momentum and heat transfer, respectively. These two variables can be calculated using universal functions and the mathematical forms of the correction terms are as follows (Högström, 1996); Paulson, 1970).

For stable conditions:

https://doi.org/10.5194/essd-2022-195
Preprint. Discussion started: 3 August 2022

$$\psi_m = -5.3\frac{(z_m - z_{0m})}{L} \tag{8}$$

$$\psi_h = -8.0\frac{z_h - z_{0h}}{L} \tag{9}$$

For unstable conditions:

$$\psi_m = 2\ln\left(\frac{1+x}{1+x_o}\right) + \ln\left(\frac{1+x^2}{1+x_o^2}\right) - 2\tan^{-1}x + 2\tan^{-1}x_o \tag{10}$$

$$\psi_h = 2\ln\left(\frac{1+y}{1+y_o}\right) \tag{11}$$

For neutral conditions:

$$\psi_m = \psi_h = 0 \tag{12}$$

In Eqs. (8–12), $x = (1 - z_m/L)^{0.25}$, $x_o = (1 - z_{om}/L)^{0.25}$, $y = (1 - 11.6z_h/L)^{0.5}$, and $y_o = (1 - 11.6z_{oh}/L)^{0.5}$. $L = T_a u_*^2/(kgT_*)$ and is defined as the Obukhov length (m), where g = 9.8 m/s^2 and T* is the fractional temperature (K). $T^* = -(\theta_s - \theta_a)/(\ln(z_h/z_{oh}) - \psi_h)$, where θ_s can be approximated using the LST and $\theta_a = T_a + z_h \cdot g/C_p$ is the potential temperature (K). The parameterization of u_* and L has also been successfully applied on the TP (Chen, et al., 2013; Su et al., 2002). In Eq. (13), z_{oh} is the roughness length of the heat transfer (m). An efficient parameterization scheme for z_{oh} has been widely applied in remote sensing land surface fluxes and land surface models (LSMs) over the TP (Biermann et al., 2014; Chen et al., 2013; Ma et al., 2015). This scheme was also applied in this study:

$$z_{0h} = \frac{70v}{u_*}\exp\left(-7.2u_*^{0.5}|T_*|^{0.25}\right) \tag{13}$$

where v is the fluid kinematic viscosity ($1.328 \cdot 10^{-5} \cdot (P_0/P_a) \cdot (T_a/T_0)^{1.754}$), where P_0 = 1013 hPa and T_0 = 273.15 K. The MOD16-STM model also considers the impacts of the soil classification and soil texture on the soil porosity (θ_{sat}), based on which the water saturation degree of surface soil (θ/θ_{sat}) is used to constrain the evaporation resistance (r_s) and E_s estimates as follows:

$$r_s = \exp\left(a + b \times \frac{SM}{\theta_{sat}}\right) \tag{14}$$

where a and b are empirical parameters for different soil textures (Table B2 and Fig. B1). The θ_{sat} estimated considering the soil organic content (*SOC*) and gravel content can be obtained from the *Soc-Vg* scheme (Chen et al., 2012; Zhao et al., 2018):

https://doi.org/10.5194/essd-2022-195
Preprint. Discussion started: 3 August 2022

$$\theta_{sat} = (1 - V_{SOC} - V_g) \times \theta_{sat,m} + V_{SOC} \times \theta_{sat,sc} \tag{15}$$

where θ_{sat_m} is the porosity of the mineral soil (θ_{sat_m} = 0.489 – 0.00126% sand) (Cosby et al., 1984), and θ_{sat_sc} is the porosity of the *SOC* (0.9 m^3/m^3 in this study) (Farouki, 1981; Letts et al., 2000). V_{soc} and V_g are the volumetric fractions of the *SOC* and gravel, respectively, and they can be calculated as follows:

$$V_{SOC} = \frac{\rho_p \times (1 - \theta_{sat,m}) \times m_{SOC}}{\rho_{SOC} \times (1 - m_{SOC}) + \rho_p \times (1 - \theta_{sat,m}) \times m_{SOC} + (1 - \theta_{sat,m}) \times \dfrac{\rho_{SOC} \times m_g}{1 - m_g}} \tag{16}$$

$$V_g = \frac{\rho_{SOC} \times (1 - \theta_{sat,m}) \times m_g}{(1 - m_g) \times \left(\rho_{SOC} \times (1 - m_{SOC}) + \rho_p \times (1 - \theta_{sat,m}) \times m_{SOC} + (1 - \theta_{sat,m}) \times \dfrac{\rho_{SOC} \times m_g}{1 - m_g} \right)} \tag{17}$$

in which the mineral particle density (ρ_p) and the bulk density of the organic matter (ρ_{soc}) were defined as 2700 kg/m^3 and 130 kg/m^3, respectively, and m_{soc} and mg are the organic and gravel percentages in each soil layer, respectively.

2.2.2 Input data

The MOD16-STM model uses various remote sensing datasets, reanalysis datasets, and meteorological forcing datasets to estimate the monthly ET across the entire TP. To avoid spatial and temporal gaps in the final product, specific datasets were selected for use in this study (Table 1). The monthly meteorological forcing data from the China Meteorological Forcing Dataset (CMFD), with a 0.1° spatial resolution for 1982–2018 was obtained from the National Tibetan Plateau Data Center (Yang et al., 2010; He et al., 2020), including the wind speed (wind), air temperature (T_a), air specific humidity (q), air pressure (P_a), shortwave downward radiation (SWD), and longwave downward radiation (LWD). The land surface temperature (LST) and precipitation (Prec) of the ERA5-Land with a 0.1° spatial resolution and monthly temporal resolution were obtained from European Centre for Medium-Range Weather Forecasts (ECWMF). The albedo (α) product with a 0.05° spatial resolution and 8-day temporal resolution was produced from the Global Land Surface Satellite (GLASS) (Liang et al., 2021). A long-term normalized difference vegetation index (NDVI) dataset with a 0.05° spatial resolution and daily temporal resolution were domwnload from the National Oceanic and Atmospheric Administration's National Centers for Environmental Information (NOAA-NCEI) and was used to calculated the canopy height and LAI (Chen et al., 2013). A topsoil moisture (0–10 cm) dataset with a 0.25° spatial resolution and monthly temporal resolution was obtained from the Global Land Evaporation Amsterdam Model (GLEAM) (Miralles et al., 2011). This dataset has been validated to perform well across the TP (Liu et al., 2021). The upward surface longwave radiation (LWU) was derived from the

https://doi.org/10.5194/essd-2022-195
Preprint. Discussion started: 3 August 2022

LST using the Stefan-Boltzmann Law. The emissivities (ε) of the mixed pixels were calculated using the specific emissivities of the vegetated (ε_v) and bare (ε_s) land surfaces, following Sobrino et al. (2004). The Harmonized World Soil Database v1.2 (HWSD) provides reliable soil texture and soil property data (Wieder et al., 2014). These data were used to calculate the soil evaporation resistance. The spatial resolutions of all of the inputs were interpolated to a 0.01° spatial resolution using a widely used bilinear interpolation method.

Table 1. Input datasets used to calculate the ET on the Tibetan Plateau.

	Data source	Temporal resolution	Availability	Spatial resolution	Method
SWD	CMFD	3 h	1979–2018	0.1° × 0.1°	Reanalysis
LWD	CMFD	3 h	1979–2018	0.1° × 0.1°	Reanalysis
T_a	CMFD	3 h	1979–2018	0.1° × 0.1°	Reanalysis
q	CMFD	3 h	1979–2018	0.1° × 0.1°	Reanalysis
Wind speed	CMFD	3 h	1979–2018	0.1° × 0.1°	Reanalysis
P_a	CMFD	3 h	1979–2018	0.1° × 0.1°	Reanalysis
LST	ERA5	Monthly	1981–2021	0.1° × 0.1°	Reanalysis
α	GLASS	8 days	1981–2019	0.05° × 0.05°	Satellite
NDVI	AVHRR	Daily	1981–2019	0.05° × 0.05°	Satellite
SM	GLEAM	Monthly	1979–2019	0.25° x 0.25°	Reanalysis
Soil Properties	HWSD	/	/	0.083°/1 km	/

2.3 Validation methods

2.3.1 Point-scale validation

The MOD16-STM model has been validated using 10 soil textures (loam, silt loam, sandy loam, sand, loamy sand, clay loam, silty clay loam, silty clay, and clay) for independent sites with three surface cover types (grassland, evergreen forest, and cropland) (Appendix A). Furthermore, the ET estimation needed to be validated through comparison with independent flux tower observations. In this study, hourly flux data measured by EC towers at nine stations (Table 2) of the China-Flux (Dang-Xiong site (DX), Hai-Bei site (HB), Yu et al., 2006; Zhang et al., 2019a), the Tibetan Observation and Research Platform (TORP) (BJ, NADORS, SETORS, QOMS, NAMORS, and Shuang-Hu (SH), Ma et al., 2020), and the Heihe Water Watershed Allied Telemetry Experimental Research (HiWATER)

(Arou, Liu et al., 2011, 2018; Che et al., 2019) networks, were also evaluated and used to validate the modeled ET. The locations of these stations had three land cover types (grassland, alpine steppe, and Gobi). It should also be noted that the energy balance closure ratio (ECR) means that the sum of sensible heat (H), latent heat (LE) and soil heat flux (G0) does not equal net radiation (Rn). Therefore, EC measurements should be screened and corrected beforehand. Half-hour LE data was corrected using Bowen ratio energy balance correction (Eq. (19)) (Chen et al., 2014).

Table 2. Details of the nine flux observation stations.

Sites	Long., Lat.	Land cover type	Elevation (m)	Availability	Climate zone
Shuang-Hu (SH)	88.83°E, 33.21°N	Grassland	4947	2013–2018	Semi-arid
BJ	91.90°E, 31.37°N	Alpine steppe	4509	2010–2016	Semi-arid
NADORS	79.60°E, 33.38°N	Grassland	4264	2010–2018	Arid
SETORS	94.73°E, 29.77°N	Grassland	3326	2007–2018	Sub-humid
QOMS	86.95°E, 28.35°N	Gobi	4276	2007–2018	Semi-arid
NAMORS	90.99°E, 30.77°N	Grassland	4730	2008–2018	Semi-arid
Arou	100.46°E, 38.05°N	Grassland	3033	2008–2017	Sub-humid
Dang-Xiong (DX)	91.06°E, 30.49°N	Grassland	2957	2004–2010	Semi-arid
Hai-Bei (HB)	101.32°E, 37.61°N	Grassland	3190	2002–2010	Sub-humid

$$ECR = \frac{H + LE}{R_n - G_0} \tag{18}$$

$$LE_{cor} = \frac{R_n - G_0}{H + LE} \times LE \tag{19}$$

To this end, the half-hourly LE_{cor} data for all of the different sites were processed to produce daily and monthly averages, using a quality control procedure. The daily average values derived from valid numbers less than 80% of the half-hourly flux in one dataset were set as null values. Similarly, the monthly average values derived from numbers less than 80% of the daily data in each month were not used in the validation.

2.3.2 Accuracy estimation

The flux tower measurements (G_i) were compared with the estimates (M_i) to evaluate the performances of the model and product. The coefficient of determination (R^2), mean bias (MB), root mean square error (RMSE), and index of agreement (IOA) were selected to assess the accuracy of the modeled ET. The equations for these parameters are as follows:

$$R^2 = \frac{\left(\sum_{i=1}^{n}(M_i - \overline{M})(G_i - \overline{G})\right)^2}{\sum_{i=1}^{n}(M_i - \overline{M})^2 \sum_{i=1}^{n}(G_i - \overline{G})^2}, 0 \le R^2 \le 1 \tag{20}$$

$$MB = \frac{1}{N}\sum_{i=1}^{n}(M_i - G_i) \tag{21}$$

$$RMSE = \sqrt{\frac{1}{n}\sum_{i=1}^{n}(M_i - G_i)^2} \tag{22}$$

$$IOA = 1 - \frac{\sum_{i=1}^{n}(M_i - G_i)^2}{\sum_{i=1}^{n}(|M_i - \overline{G}| + |G_i - \overline{G}|)^2} \tag{23}$$

where $\overline{G}$ and $\overline{M}$ are the mean flux tower and simulated ET values, respectively, the subscript i denotes the ith sample, and n is the number of samples. The R^2 value was calculated to evaluate the linear relationship between the modeled and observed ET. A higher R^2 value indicates a higher correlation. The MB was used to assess whether the result was overestimated (positive MB values) or underestimated (negative MB values). The RMSE was used to evaluate the performance of the model. A smaller RMSE indicates a higher accuracy. The IOA quantifies the degree to which the simulated ET and flux tower are correlated to each other, with values between 0 and 1.

3. Results

3.1 Evaluation of ET products against flux tower measurements

The reliability of the remote sensing-based ET estimates is questionable in the absence of verification using ground measurements. For every EC site on the TP, we extracted the simulated monthly ET rates of the 0.01° grid where the EC flux tower was located. The validation results for the monthly MOD16-STM ET obtained using the flux tower observational data are shown in Fig. 3. Compared to the ET observations, the modeled ET exhibited a good performance and high consistency over the TP. The grassland sites (SETORS, Arou, DX, and HB) performed well, with R^2 and IOA values exceeding 0.82 and 0.95. The NAMORS site performed the poorest, with the highest RMSE (17.84 mm/month) and the lowest R^2 and IOA (0.63 and 0.87, respectively). On average, the mean R^2 and IOA values were greater than 0.83 and 0.93. The R^2 values all passed the significance test at the $p < 0.05$ level. The mean |MB| and RMSE values were less than 3 mm/month and 14 mm/month. It should be noted that the fact that MB was greater than 0 revealed that the ET was overestimated, especially during the dry season over the barren land (QOMS, DX, SH, and NADORS) (Fig. 3). Fig. 4 shows the time series of the variations in the ET. In general, both the MOD16-STM ET and observed ET exhibited clear seasonal variation characteristics at the nine flux tower stations. Moreover, an annual periodic variation was observed at most stations. The site-scale validation demonstrates that the MOD16-STM ET has a satisfying accuracy in the TP region.

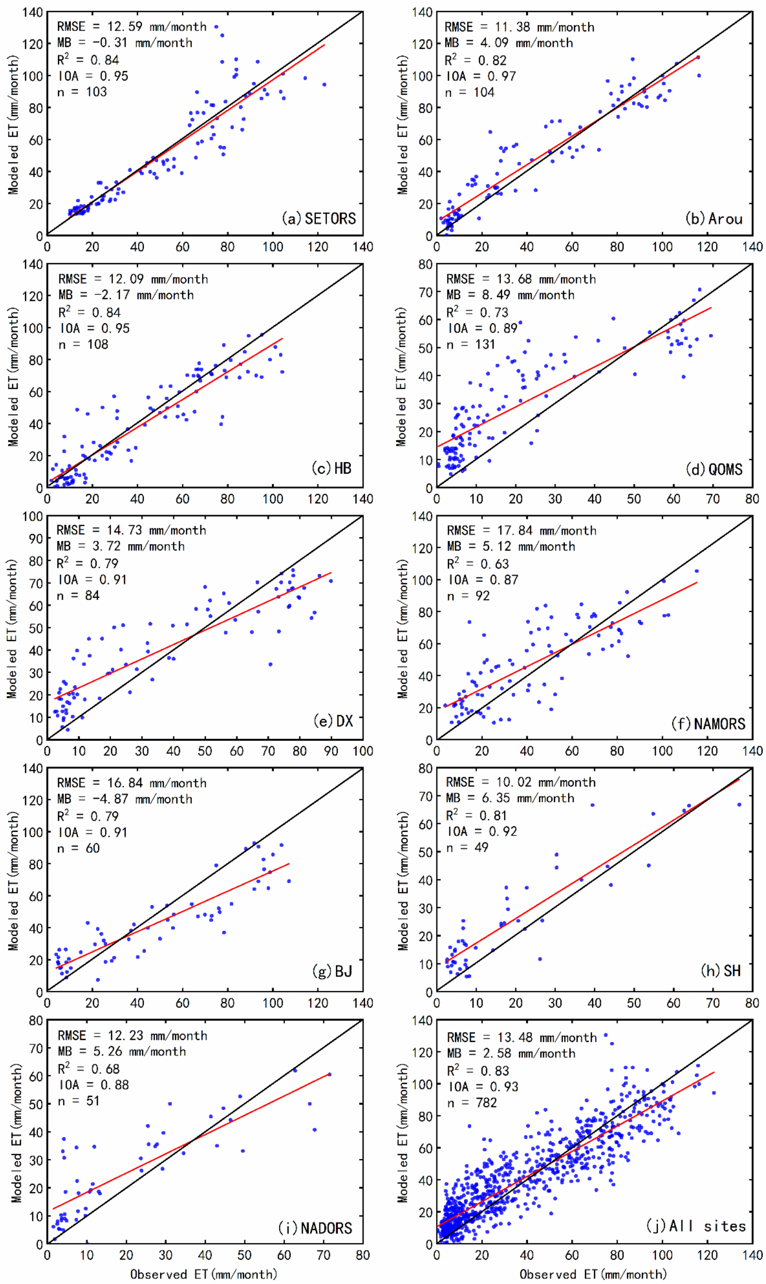

Figure 3 The validation of the MOD16-STM monthly ET at (a) SETORS, (b) Arou, (c) HB, (d) QOMS, (e)
260 DX, (f) NAMORS, (g) BJ, (h) SH, (i) NADORS, and (j) all sites.

https://doi.org/10.5194/essd-2022-195
Preprint. Discussion started: 3 August 2022

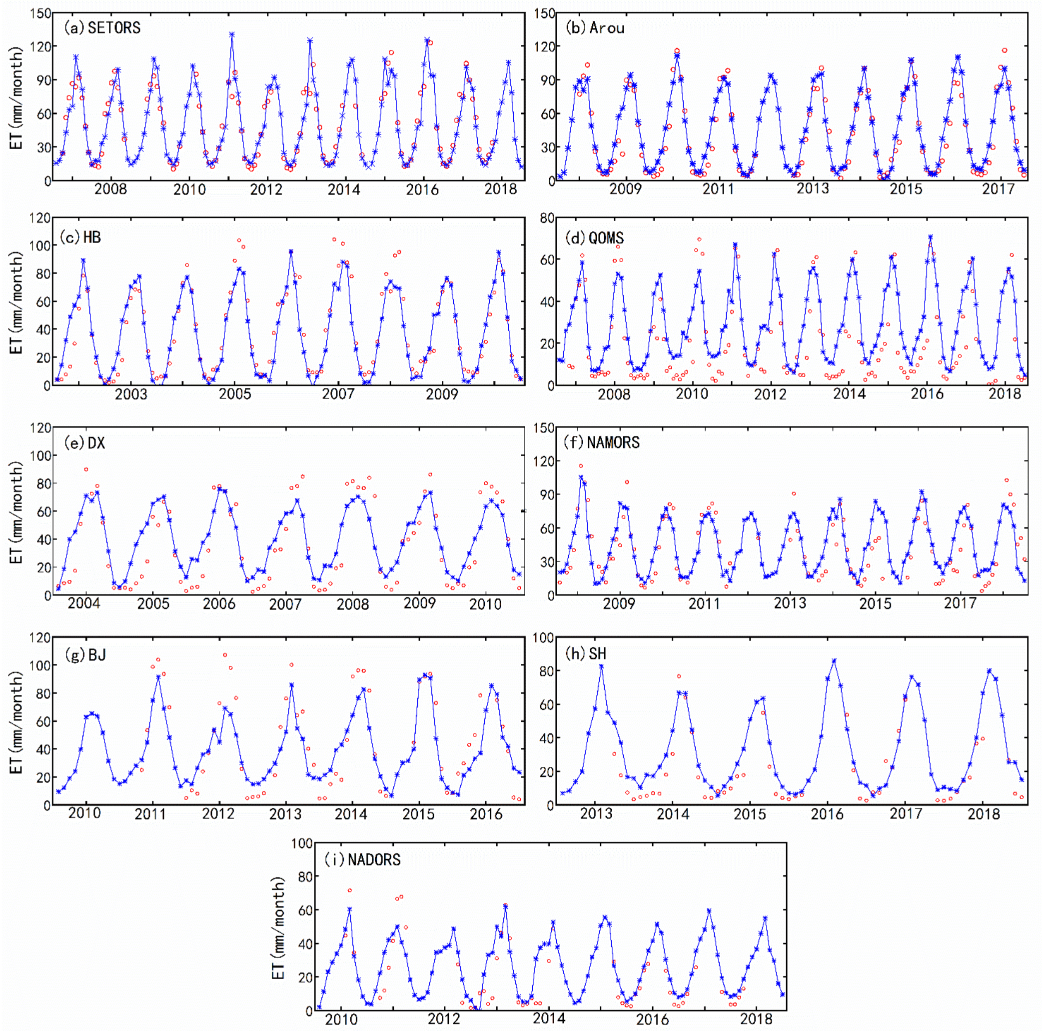

Figure 4 Time series variations in the MOD16-STM simulated ET and flux-tower-observed ET at (a) SETORS, (b) Arou, (c) HB, (d) QOMS, (e) DX, (f) NAMORS, (g) BJ, (h) SH, and (i) NADORS.

265

https://doi.org/10.5194/essd-2022-195
Preprint. Discussion started: 3 August 2022

3.2 Spatial pattern of the multiyear averaged ET across TP

Fig. 5 shows the spatial pattern of the multiyear (1982–2018) average ET and its three components across the TP. The ET decreased from southeast to northwest, with the maximum values exceeding 1000 mm/year on the southeastern Tibetan Plateau (the Heng-duan Mountains) and minimum values of less than 100 mm/year in the Qaidam Basin and northwestern TP. The spatial pattern of the annual ET was consistent with that of the aridity index (AI) (Fig. 1b), which is due to the combined effect of the atmospheric demand and water supply. The ET of the sub-humid zone (32.9% of the TP) contributed the highest percentage (43% of the TP's ET) compared to the other climate zones. The E_s obviously dominated on the central and western TP, and its spatial distribution pattern was very similar to that of the ET. The spatial distributions of the E_c and E_w were consistent with the spatial distribution of the vegetation. The high E_c (>200 mm/year) and E_w (>50 mm/year) values were mainly concentrated in the densely vegetated areas of the Heng-duan Mountains on the southeastern TP.

The multiyear-average ET in spring (March, April, and May), summer (June, July, and August), autumn (September, October, and November), and winter (December, January, and February) on the TP are shown in Fig. 6. The estimated ET seems to capture the general pattern of the seasonal cycles relatively well. The average ET was higher in spring than in autumn. The ET ranged from 20 to 250 mm in spring and from 20 to 150 mm in autumn. This is attributed to the fact that as the ground surface increases with increasing temperature in spring, more free surface water is generated via thawing of the permafrost and melting of snow and ice, which enhances the surface evaporation processes. In addition, vegetation transpiration increases during the growing season. In summer, the ET is greater than 200 mm over most of the TP, but the ET is still less than 100 mm in large areas of the northwestern TP. However, lower ET values were only observed in the densely vegetated southeastern region of the TP in winter due to the lower amount of available water (precipitation) and lower T_a throughout the entire TP.

The multi-year average land surface ET over the TP was 346.5 ± 13.2 mm/year (mean ± standard deviation, the latter represents the interannual variability) (about 0.88 ± 0.034 Gt/year), with E_s equal to 292.36 ± 10.39 mm/year (0.74 ± 0.027 Gt/year), E_c equal to 47.85 ± 3.34 mm/year (0.12 ± 0.006 Gt/year), and E_w equal to 7.07 ± 2.89 mm/year (0.02 ± 0.001 Gt/year). The multi-year mean annual E_s accounted for the majority of the ET on the TP (more than 84%). Wang et al. (2020) accurately calculated the amount of water evaporated from all of the plateau lakes, i.e., 0.0517 Gt/year. Thus, the average annual water evaporated on the entire TP was calculated using the area-weighted average of about 0.93 ± 0.037 Gt/year. About 53% of the precipitation on the Tibetan Plateau (according to the ERA5-Land precipitation data, the average annual rainfall on the TP is about 1.8×10^3 Gt/year) returns to the atmosphere through ET. The multiyear seasonal ET averaged over the entire TP is 90.79 ± 3.16 mm/year (0.23 ± 0.0081 Gt/year),

https://doi.org/10.5194/essd-2022-195
Preprint. Discussion started: 3 August 2022

152.05 ± 8.44 mm/year (0.38 ± 0.021 Gt/year), 71.96 ± 2.86 mm/year (0.18 ± 0.0074 Gt/year), and 30.54 ± 1.85 mm/year (0.077 ± 0.0047 Gt/year) in spring, summer, autumn, and winter, respectively.

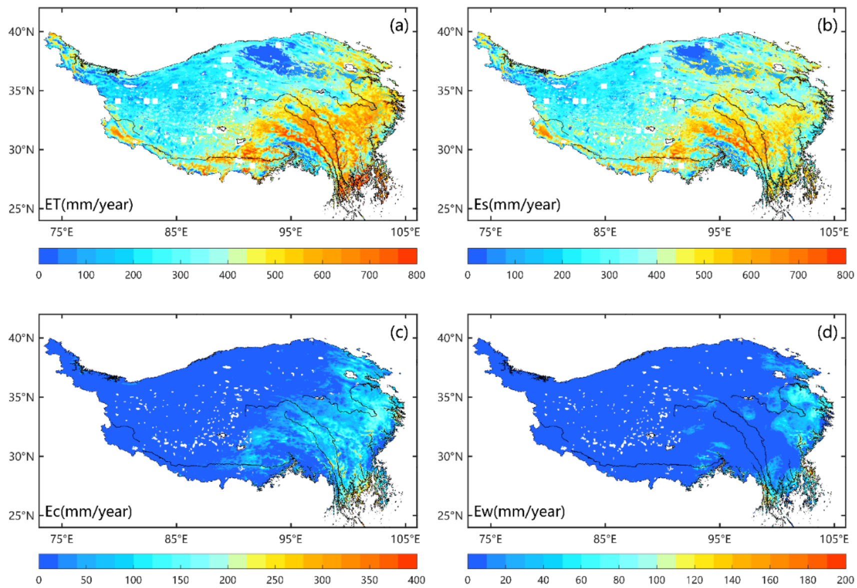

Figure 5 Spatial pattern of the multiyear (1982–2018) mean annual (a) ET, (b) E_s, (c) E_c, and (d) E_w across the Tibetan Plateau.

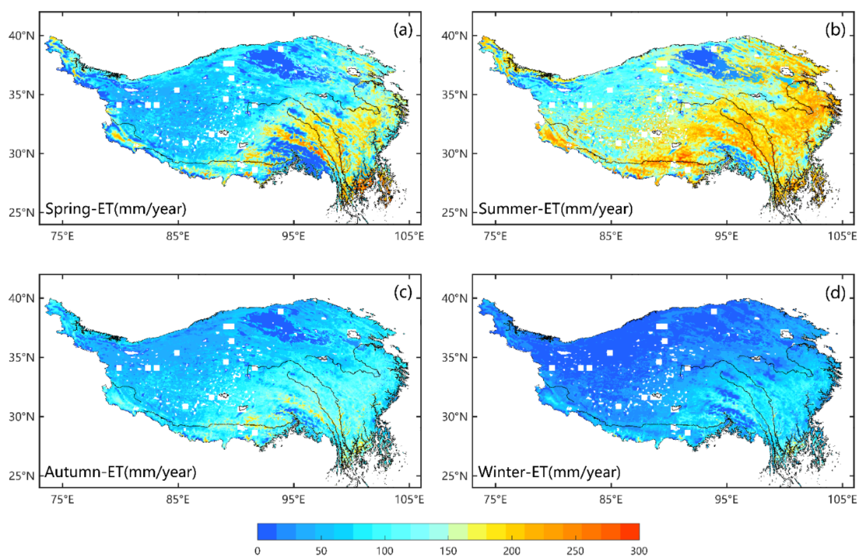

Figure 6 Spatial distributions of the multiyear (1982–2016) mean seasonal ET in (a) Spring, (b) Summer, (c) Autumn, and (d) Winter across the Tibetan Plateau.

https://doi.org/10.5194/essd-2022-195
Preprint. Discussion started: 3 August 2022

3.3 Temporal variations in ET across TP

Quantifying the inter- and intra-annual variations in the land surface energy variables is important in studying monsoon phenomena and climate change. Fig. 7 shows the spatial patterns of the annual ET and its components, as well as their rates, during 1982–2018 across the TP. The trends of the ET are spatially heterogeneous over the TP. The annual ET significantly increased, with rates of about 1–4 mm/year ($p < 0.05$), over most parts of the central and eastern TP, accounting for more than 86% of the TP. However, it significantly decreased, with rates of −3 to −1 mm/year, on the northwestern TP. In addition, the E_s rates exhibited a spatial distribution similar to that of the ET, and the increasing trends had lower magnitudes (1–3 mm/year, $p < 0.05$). Both the E_c and E_w exhibited slightly increasing trends of 0–2 mm/year ($p < 0.05$). Averaged across the entire TP, the ET, E_s, and E_c increased significantly during 1982–2018, with rates of 0.96 mm/year, 0.64 mm/year, and 0.44 mm/year, respectively ($p < 0.05$; Fig. 8). Regarding the seasonality, the seasonal ET trends were positive and significant in all of the seasons (Fig. 8). The strongest trends occurred in summer (0.46 mm/year). In addition, the multi-source ET products indicate that most of the regions of the TP exhibited consistent ET changes over the past 30 years (Yin et al., 2013; Peng et al., 2016; Wang et al., 2018; Ma et al., 2019; Wang et al., 2020; Li et al., 2021; Ma et al., 2022).

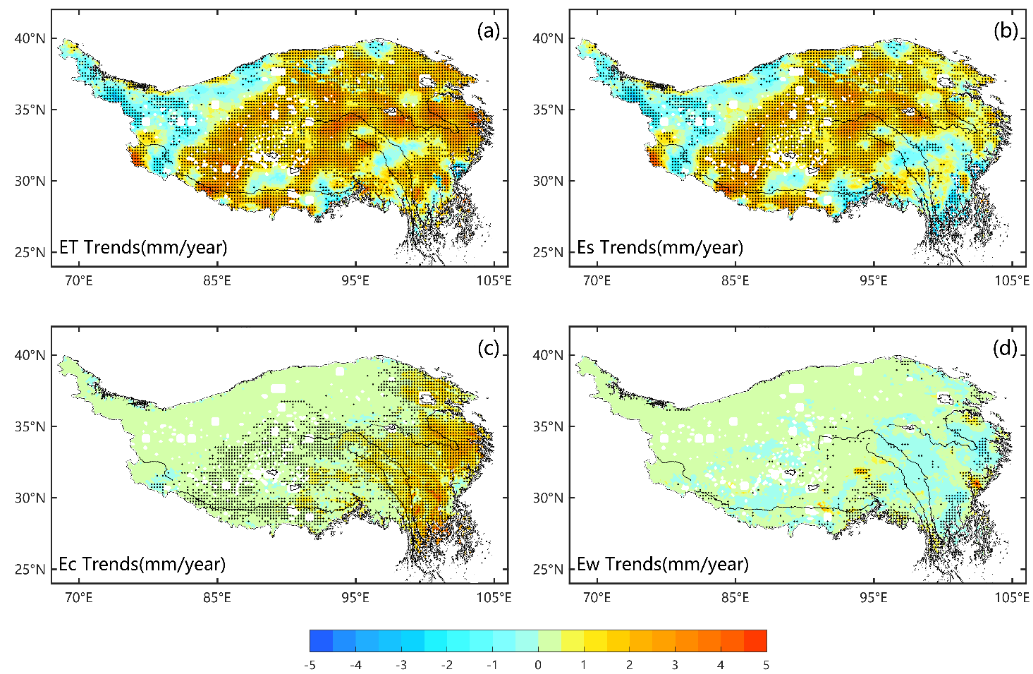

Figure 7 Spatial patterns of the trends (1982–2018) of the annual (a) ET, (b) E_s, (c) E_c, and (d) E_w across the Tibetan Plateau. The stippling on the maps indicates the trends that are statistically significant (p<0.05).

https://doi.org/10.5194/essd-2022-195
Preprint. Discussion started: 3 August 2022

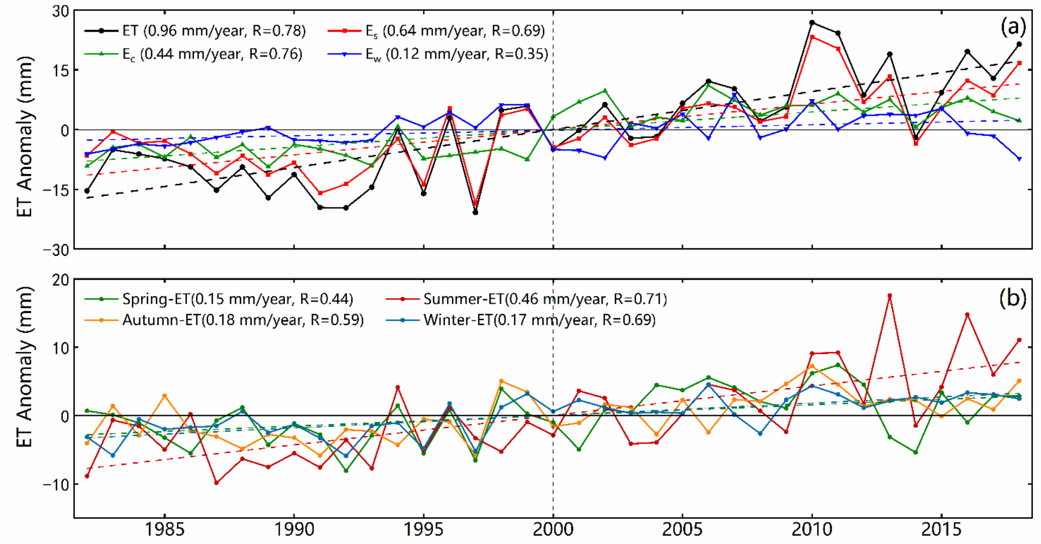

Figure 8 Time series of the (a) annual anomalies in the ET and its components and (b) seasonal anomalies in the ET and their least squares fitted linear trend.

The increase in the ET over the entire TP from 1982 to 2018 can be explained by the warming and wetting of the climate on the TP during this period. Since the 1980s, the TP has experienced overall greening, warming, and wetting and increased precipitation (Fig. 9). The ET has continuously increase in the past 40 years, while the changes in the climate factors shifted significantly in the middle of this time period (around 2000). From 1982 to 2000, the ET continuously increase, the wind speed rapidly decreased, and did not change the R_n significantly. There was a rapid decrease in the R_n and no significant change in the wind speed from 2000 to 2018, while the ET continued to increase during this period. Therefore, the R_n and wind speed were not the dominant factors controlling the annual variations in the ET. The significant increases in the T_a, SM, and precipitation were accompanied by greening of the land surface in the last two decades. Together, these factors led to an increase in the ET. In the following ten years, only the significant growth of the SM controlled the growth of the ET.

In general, the increase in ET over the TP was due to the increase in the available surface water during the entire study period. There is also evidence that an overall increase in precipitation occurred across the TP. The combined effect of the warming and vegetation greening led to further opening of the vegetation stomata. The more favorable vegetation conditions explain the increase in the vegetation transpiration. The warming of the land surface and increased wind speeds led to more efficient turbulent water exchange between the land and atmosphere. In addition, the warming accelerated the melting of the permafrost and glaciers on the TP. Due to the wetting of the surface and

https://doi.org/10.5194/essd-2022-195
Preprint. Discussion started: 3 August 2022

the thickening of the active soil layer, water could be transported more easily from the lower layer to the upper soil

345 layer.

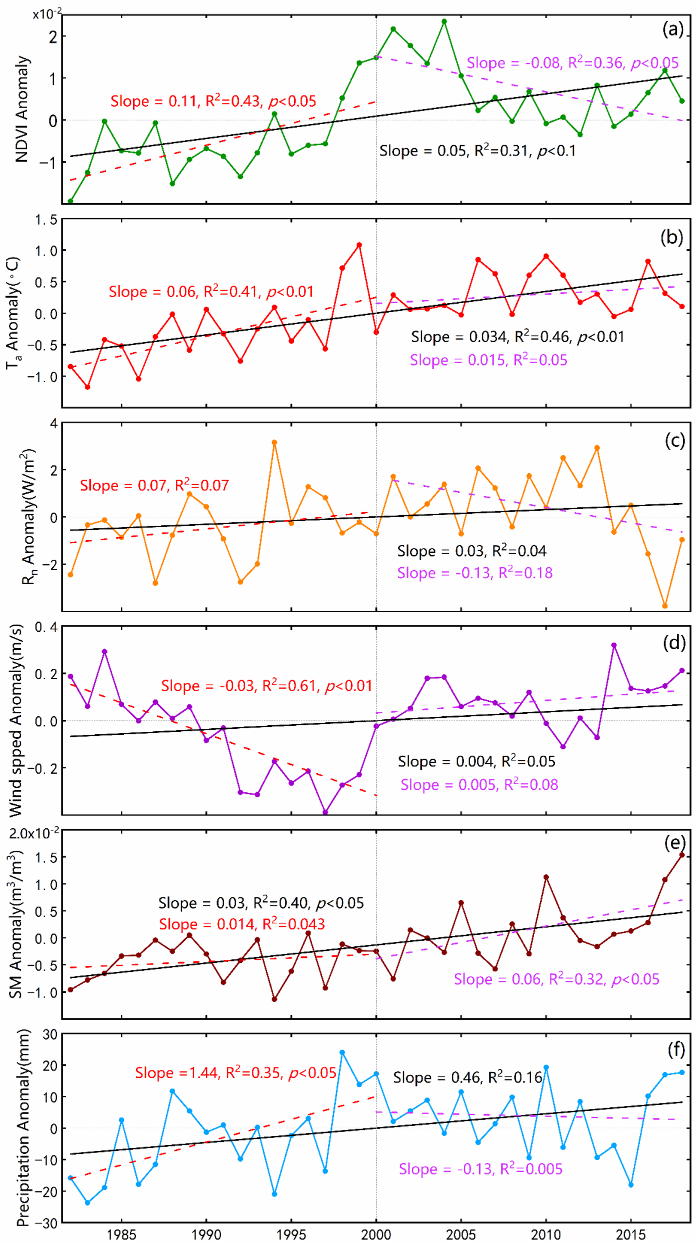

Figure 9 Time series of the annual anomalies in the (a) NDVI, (b) T_a, (c) R_n, (d) u, (e) SM, and (f) Precipitation and their least squares fitted linear trends for different time periods.

Open Access Earth System Science Data Discussions

3.4 comparison of the MOD16-STM product to other ET product over the TP

The MOD16-STM ET had a relatively good performance on the TP overall, with an average R^2 value of 0.83 and an average RMSE of 13.48 mm/month. These results are close to those obtained in other studies. Wang et al. (2018) evaluated the performance of the use of a modified PML model for ET estimation (PML-Wang) based on flux tower observation data for the TP. Their results yielded R^2 values of >0.85 and RMSE values of <0.006 mm/day. The spatially averaged ET during 1982–2012 was 378.1 mm/year. Wang et al. (2020) evaluated the performance of the generalized nonlinear complementary principle for ET estimation (CR-Wang) based on flux tower observation data for the TP. Their results showed that the R^2 increased from 0.87 to 0.93, and the RMSE decreased from 0.53 to 0.40 mm/day. The spatially averaged ET during 1982–2014 was 398.3 mm/year. Han et al. (2021) used an algorithm for the effective aerodynamic roughness length of the parameterize sub-grid-scale topographic form drag coupled with the SEBS model to improve the skill of estimating the surface energy budget in the mountainous regions of the TP, and they estimated the ET (Han-ET) for the entire TP from 2001 to 2018. They found that the modeled value was very consistent with the in situ measured value ($R^2 > 0.81$, RMSE < 14.5 mm/month), but their value was slightly lower than that obtained in this study. In addition, the average annual ET (496 ± 23 mm) on the TP that they obtained was also higher than that obtained in this study (346.5 ± 13.2 mm). This discrepancy is mainly due to the different models and time periods of the two studies. Ma et al. (2022) used PML_V2 to estimate the ET (PML-Ma) on the TP, and their R^2 and RMSE values varied from 0.4 to 0.9 and from 0.3 to 0.8 mm/day, respectively. The 35-year mean annual ET rates led to an average value of 353 ± 24 mm/year for the entire TP. Soil evaporation is the main component (64%) of the ET. The main reason this ratio is inconsistent with the results of this study is because of the differences in the land cover classification. The land cover of the MODIS largely classifies the land surface of the northwestern TP as bare soil, which leads to an increase in the proportion of soil evaporation.

4. Discussion

4.1 Evaporated water across the TP

Yao et al. (2013) estimated the ET (PT-Yao) in China using a satellite-driven modified Priestley–Taylor algorithm, which is constrained by the NDVI and the apparent thermal inertia derived from the temperature changes over time, and they reported that the mean annual ET on the TP was about 320 mm/year. Song et al. (2017) estimated TP's ET (PM-Song) using the improved Penman–Monteith method and meteorological and satellite remote sensing data with a spatial resolution of 1 km during 2000–2010, and they concluded that the average annual ET on the TP was 350.3 mm/year. In addition to this, the 18 mean annual ET values on the TP estimated using existing multi-source ET products (PML-Zhang (Zhang et al., 2019b), EB-ET (Chen et., 2019, 2021), CR-Ma (Ma et al., 2019), CMIP6-

https://doi.org/10.5194/essd-2022-195
Preprint. Discussion started: 3 August 2022

ssp126 (Eyring et al., 2016), GLDAS-Noah (Rodell et al., 2004), GLASS (Liang et al., 2021), GLEAM-v3.5b (Miralles et al., 2011), and ERAR-Land (Muñoz-Sabater et al., 2021)) and previous research results (MTE (Jung et al., 2010), PM-Li (Li et al., 2014a), LPJ-Yin (Yin et al., 2013)) are listed in Table 3 and shown in Fig. 10. The results show the large differences in the estimated mean annual ET values for the TP. The Han-ET, ERA5-Land, and CMIP6 produced the highest values (>400 mm/year), while the LPJ-Yin, GLASS, EB-ET, GLDAS, and GLEAM values were less than 300 mm/year. The differences in these results are partially caused by objective factors such as the inaccuracy of the input data and the limitations of the validation methods. In addition, the subjective factor of the algorithm's flaws led to additional biases. The medium value of the annual ET from an ensemble of datasets is 348.6 mm/year. This is the closest to the result (346.5 mm/year) estimated in this study using the MOD16-STM model. Overall, the MOD16-STM ET exhibited acceptable performance on the TP, which was demonstrated by the above comparison with previous studies.

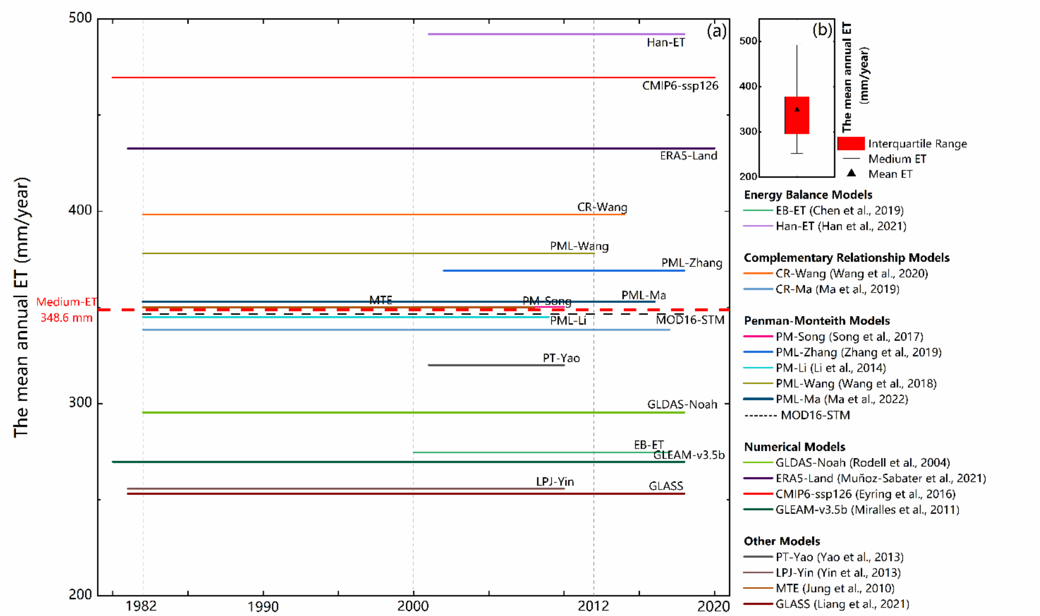

Figure 10 (a) (a) The annual mean ET values of 18 datasets. The *x*-axis is the time coverage of the ET datasets, and the *y*-axis is the multi-year mean value. (b) The bars denote the mean values and variations of the annual ET.

https://doi.org/10.5194/essd-2022-195
Preprint. Discussion started: 3 August 2022

Open Access Earth System Science Data Discussions

Table 3 Annual mean evapotranspiration values and trends for regions of the Tibetan Plateau.

Dataset	Method	Period	Length (year)	Mean ET (mm)	ET trend (mm/year)	Reference
PT-Yao	Modified Priestley −Taylor model	2001-2010	10	320.0	-0.14	Yao et al. (2013)
PM-Song	Penman-Monteith (PM) method	2000-2010	11	350.3	-4.69	Song et al. (2017)
PML-Zhang	Penman-Monteith-Leuning (PML) model	2002-2018	17	369.2	5.01	Zhang et al. (2019b)
EB-ET	Energy balance model	2000-2017	18	274.6	-1.66	Chen et al.(2019, 2021)
Han-ET	Energy balance model	2001-2018	18	492.1	-1.52	Han et al. (2021)
MTE	Model tree Ensembles	1982-2008	27	350.0	/	Jung et al. (2010)
PM-Li	Penman-Monteith (PM) model	1982-2009	28	345.0	/	Li et al. (2014a)
LPJ-Yin	Lund-Potsdam-Jena dynamic vegetation model	1981-2010	30	255.8	0.08	Yin et al. (2013)
PML-Wang	Penman-Monteith-Leuning (PML) model	1982-2012	31	378.1	/	Wang et al. (2018)
PML-Ma	Penman-Monteith-Leuning (PML) model	1982-2016	35	353	1.87	Ma et al. (2022)
CR-Wang	C-R (complementary relationship) model	1982-2014	32	398.3	0.77	Wang et al. (2020)
CR-Ma	C-R (complementary relationship) model	1982-2017	36	338.4	0.82	Ma et al. (2019)
CMIP6-ssp126	Global climate model	1982-2018	37	456.6	0.48	Eyring et al. (2016)
GLDAS-Noah	Land surface data assimilation	1982-2018	37	295.4	1.10	Rodell et al. (2004)
MOD16-STM	Penman-Monteith (PM) method	1982-2018	37	346.5	0.96	In this study
GLASS	Empirical method	1981-2018	38	253.2	0.53	Liang et al. (2021)
GLEAM-v3.5b	Microwave remote sensing data assimilation	1980-2018	39	269.7	0.94	Miralles et al. (2011)
ERA5-Land	Reanalysis	1981-2020	40	432.7	0.68	Muñoz-Sabater et al. (2021)
Medium-ET	/	/	/	348.6	/	/

4.2 Errors caused by objective factors

The MOD16-STM and other models use remote sensing data and reanalysis data as the main input data. However, the accuracy of these data is somewhat uncertain (Ramoelo et al., 2014). For instance, the topsoil water content is a critical radiative parameter; however, complex algorithm-led reanalysis data SM products can contain errors. Liu et al. (2021) reported that the long-term GLEAM SM product based on a satellite-based input dataset yields limited improvement in its SM outputs and the data assimilation model does not perform well. Furthermore, as a fundamental parameter in the calculation of the surface energy balance, the LST affects the estimation of the ET to a great extent

https://doi.org/10.5194/essd-2022-195
Preprint. Discussion started: 3 August 2022

(Long et al., 2011). In this study, we used an NDVI threshold to divide the bare soil evaporation and mixed pixel ET, which largely overestimated the soil evaporation. The mismatch in the underlying surface heterogeneity and the spatial resolution of the flux column of the MOD16-STM ET can also lead to errors. In general, the flux towers covered areas ranging from a few hundred square meters to several square kilometers, depending on the height of the observation instrument, the turbulence intensity, topography, environment, and vegetation conditions. Although site evaluations of the MOD16-STM ET were performed in this study, the uncertainties arising from the limited number of validation sites should be noted, and validation with different land cover types, climate zones, elevations, and seasons should be considered.

5. Conclusion

In this study, we developed a 37-year (1982–2018) monthly ET dataset with a 0.01° spatial resolution for the TP using the newly developed MOD16-STM model coupled with soil information to investigate the spatial distribution and temporal trends of the ET on the TP. Although previous studies have been conducted on the ET climatology on the TP (Peng et al., 2016; Wang et al., 2018; Ma et al., 2019; Wang et al., 2020; Li et al., 2021; Han et al., 2021; Ma et al., 2022), this is also a suitable ET database for use in climate studies covering the full study area with a high spatial resolution and a long time period. Our main findings are summarized below.

1. The ET product generated using MOD16-STM exhibited a good performance on the TP. Compared to the flux tower observation data, the R^2 and IOA values of the modeled ET reached 0.83 and 0.93 for 782 samples, and the RMSE was 13.48 mm/month. MOD16-STM overestimated the ET overall, with an MB of 2.58 mm/month. The MOD16-STM ET product can adequately represent the actual ET and can be used in research in water resource management, drought monitoring, and ecological change.
2. The combined effect of the atmospheric demand and water supply resulted in spatial heterogeneity of the ET and the changes in the ET. The annual ET generally decreased from southeast to northwest on the TP. The E^s accounted for more than 84% of the annual ET. The estimated multiyear (1982–2018) mean annual ET on the TP was 346.5±13.2 mm, resulting in approximately 0.93 ± 0.037 Gt/year of total water evapotranspiration from the entire TP.
3. The ET exhibited a significant increasing trend, with rates of about 1 to 4 mm/year ($p<0.05$), over most parts of the central and eastern TP and a significant decreasing trend, with rates of −3 to −1 mm/year, on the northwestern TP. Averaged across the entire TP, the ET increased significantly during 1982–2018, with a rate of 0.96 mm/year. The increase in the ET over the entire TP from 1982 to 2018 can be explained by the warming and wetting of the climate during this period.

https://doi.org/10.5194/essd-2022-195
Preprint. Discussion started: 3 August 2022

The MOD16-STM ET product exhibited a high degree of agreement with the results of the latest studies of the ET on the TP, and our results have a longer time series and higher spatial and temporal resolutions. However, there are still large errors at the point scale. The MOD16-STM algorithm has a great dependence on higher-precision soil moisture products. In this study, the empirical coefficients for the different soil textures were redefined, and the influence of the physical processes of deeper soil water and heat transfer on the resistance should be considered in the future. Thus, the improvements of the MOD16-STM algorithm will be the focus of future research. In addition, most areas of the TP are covered by permafrost and seasonally frozen soil. In particular, during the seasonal freeze-thaw period, it is difficult to grasp the dry and wet conditions of the surface. Therefore, it is necessary to use relevant models and observations to study the characteristics of the ET during the soil freeze-thaw period to verify the applicability of the model to the study of ET on the TP.

Data availability

The monthly ET dataset presented and analysed in this article has been released and is freely available at the Science Data Bank (http://doi.org/10.11922/sciencedb.00020, Y. Ma*, X.Chen*, L. Yuan, 2021) and the National Tibetan Plateau Data Center (TPDC) (http://doi.org/10.11888/Terre.tpdc.271913, L. Yuan, X.Chen*, Y. Ma*, 2021). The dataset is published under the Creative Commons Attribution 4.0 International (CC BY 4.0) license.

Author contributions

YMM, LY, and XLC led the writing of this paper and acknowledge responsibility for the experimental data and results. LY and YMM drafted the paper, and LY led the consolidation of the input and simulation dataset. This paper was written in cooperation with all of the co-authors.

Declaration of Competing Interest

The authors declare that they have no known competing financial interests or personal relationships that could have appeared to influence the work reported in this paper.

Acknowledgments

We are grateful for the datasets provided by the China-Flux (http://www.chinaflux.org/), Ameri-Flux (https://ameriflux.lbl.gov/), GHG-Europe (http://www.europe-fluxdata.eu/ghg-europe), the National Tibetan Plateau Data Center (https://data.tpdc.ac.cn/zh-hans/data), the European Centre for Medium-Range Weather Forecasts

https://doi.org/10.5194/essd-2022-195
Preprint. Discussion started: 3 August 2022

(ECWMF) (https://www.ecmwf.int/), NOAA-NCEI (https://www.ncei.noaa.gov/products/climate-data-records/normalized-difference-vegetation), the Global Land Evaporation Amsterdam Model (https://www.gleam.eu/), and the National Earth System Science Data Sharing Infrastructure (http://glass-product.bnu.edu.cn/). The authors would like to thank all of their colleagues at the observation stations on the TP for their maintenance of the instruments.

Financial support

This study was funded by the Second Tibetan Plateau Scientific Expedition and Research (STEP) Program (2019QZKK0103 and 2019QZKK0105), the Strategic Priority Research Program of the Chinese Academy of Sciences (XDA20060101), the National Natural Science Foundation of China (91837208, 41975009, and 91637312), and the Key Research Program of Frontier Sciences of the Chinese Academy of Sciences (QYZDJ-SSW-DQC019).

Appendix A: MOD16-STM Parameterization and Validation

Table A1. Basic Information about the five test sites and 12 verification sites.

	Site	Lat; lon	Land cover	θ (cm)	f_{sand}	f_{clay}	m_{soc} (%)	θ_{sat}	Soil Texture	Reference
Test Sites	IT-Cas	45.07; 8.71	CRO	5	0.28	0.29	2.6	/	Clay loam	*Denef et al. (2013)*
	US-IHO	36.47; 100.62	Bare	5	0.58	0.28	/	0.53	Sandy Clay Loam	*Lemone et al.* (2007)
	US-Arm	36.61; -97.49	CRO	5	0.28	0.43	1.5	/	Clay	*Fischer et al.* (2007)
	CH-Oe2	47.29; 7.73	CRO	5	0.095	0.43	2.8	/	Silty Clay	*Alaoui and Goetz* (2008)
	US-IB2	41.84; -88.24	GRA	0~15	0.106	0.29	2.4	/	Silty clay Loam	/
Independent verification sites	US-Dk1	35.97; -79.09	GRA	10	0.48	0.09	/	0.52	Loam	*Novick et al. (2004)*
	US-Fwf	35.45; -111.77	GRA	5	0.30	0.13	3.2	/	Silt Loam	*Dore et al. (2012)*
	US-Wkg	31.74; -109.94	GRA	5	0.67	0.17	1.0	/	Sandy Loam	*Ameri-Flux*
	CA-Obs	53.98; -105.11	ENF	5	0.72	0.05	4.3	/	Sandy Loam	*Ameri-Flux*
	CA-Ojp	53.91; -104.69	ENF	5	0.94	0.03	2.5	/	Sand	*Ameri-Flux*
	CA-Ca2	49.87; -125.29	ENF	5	0.74	0.03	3.0	/	Loamy Sand	*Ameri-Flux*
	CA-Ca3	49.53; -124.90	ENF	5	0.39	0.20	4.9	/	Loam	*Ameri-Flux*
	US-Dk3	35.97; -79.09	ENF	5	0.25	0.34	2.4	/	Silt Loam	*Ameri-Flux*
	US-Fuf	35.08; -111.76	ENF	5	0.31	0.35	3.9	/	Clay Loam	*Ameri-Flux*
	US-Ib1	41.86; -88.22	CRO	2.5	0.10	0.35	1.8	/	Silty clay Loam	*Denef et al. (2013)*
	ES-ES2	39.28; -0.32	CRO	5	0.11	0.47	3.7	/	Silty Clay	*Kutsch et al. (2010)*
	IT-Bci	40.52; 14.96	CRO	5	0.32	0.46	1.5	/	Clay	*Denef et al. (2013)*

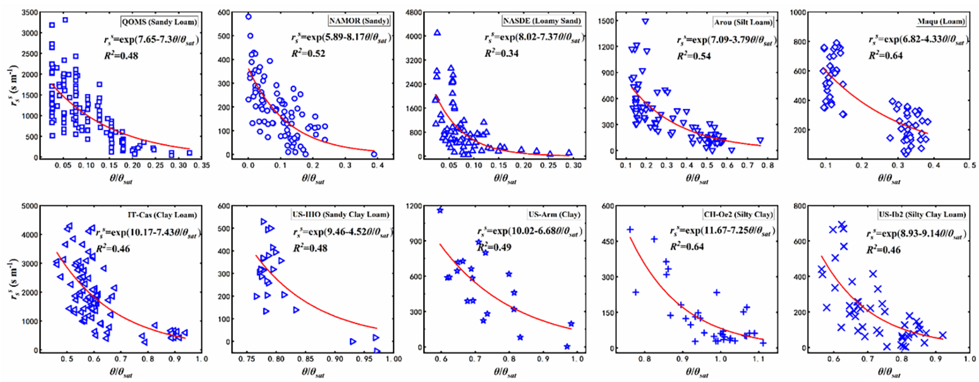

Figure A1 Soil surface resistance (r_s^s) related to the topsoil *SM* measured for the different soil textures (θsat): sandy loam (QOMS), sandy (NAMOR), loamy sand (NASDE), silt loam (Arou), loam (Maqu), clay Loam (IT-Cas), sandy clay loam (US-IHO), clay (US-Arm), silty clay (CH-Oe2), and silty clay loam (US-Ib2).

https://doi.org/10.5194/essd-2022-195
Preprint. Discussion started: 3 August 2022

Open Access Earth System Science Data Discussions

Table A2 Equation coefficient values for the surface soil resistances from the regressions between these resistances and the SM for the different soil textures (θ_{sat}).

Texture	$r_s^s = \exp\left(a + b \times \frac{SM}{\theta_{sat}}\right)$		R^2
	a	***b***	
Sandy Loam	7.65	-7.3	0.48
Sand	5.89	-8.17	0.52
Loamy Sand	8.02	-17.37	0.34
Silt Loam	7.09	-3.79	0.54
Loam	6.82	-4.33	0.64
Clay Loam	10.17	-7.43	0.46
Sandy Clay Loam	9.46	-4.52	0.48
Clay	10.02	-6.68	0.49
Silty Clay	11.67	-7.25	0.64
Silty Clay Loam	8.93	-9.14	0.46

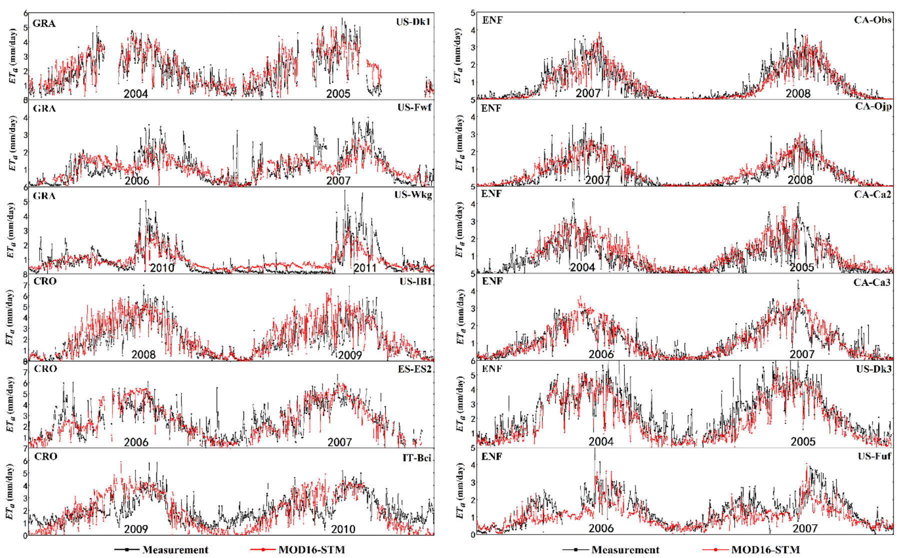

Figure A2 Time-series comparisons of the ET estimated using the MOD16-STM model and the daily flux tower observations in the grassland (US-DK1, US-Fwf, and US-Wkg), cropland (US-IB1, ES-ES2, and IT-Bci), and evergreen forest (CA-Obs, CA-Ojp, CA-Ca2, CA-Ca3, US-DK3, and US-Fuf) ecosystems.

https://doi.org/10.5194/essd-2022-195
Preprint. Discussion started: 3 August 2022

Table A3. Statistical comparison of the daily ET (mm/day) estimated using the MOD16-STM model and daily flux tower observation data.

	Sites	R^2 (p<0.05)	IOA	|MB|	RMSE
Grassland	US-DK1	0.71	0.91	0.27	0.74
	US-Fwf	0.59	0.84	0.06	0.55
	US-Wkg	0.69	0.84	0.005	0.58
Evergreen Forest	CA-Obs	0.88	0.96	0.05	0.33
	CA-Ojp	0.79	0.93	0.11	0.38
	CA-Ca2	0.77	0.92	0.23	0.49
	CA-Ca3	0.79	0.94	0.02	0.44
	US-Dk3	0.79	0.92	0.51	0.87
	US-Fuf	0.58	0.81	0.33	0.66
Cropland	US-Ib1	0.65	0.88	0.39	1.08
	ES-ES2	0.87	0.91	0.04	0.94
	IT-Bci	0.41	0.76	0.14	1.14
Mean	/	0.72	0.89	0.18	0.68

References

Alaoui, A., and Goetz, B.: Dye tracer and infiltration experiments to investigate macropore flow, Geoderma., 144(1–2), 279–286, https://doi.org/10.1016/j.geoderma.2007.11.020, 2008.

Baik, J., Liaqat, U. W., and Choi, M.: Assessment of satellite- and reanalysis-based evapotranspiration products with two blending approaches over the complex landscapes and climates of Australia, Agric. For. Meteorol., 263, 388–398. https://doi.org/10.1016/j.agrformet.2018.09.007, 2018.

Bibi, S., Wang, L., Li, X., Zhou, J., Chen, D., Yao, T.: Climatic and associated cryospheric, biospheric, and hydrological changes on the Tibetan Plateau: a review, Int. J. Climatol., 38, 1-17, https://doi.org/10.1002/joc.5411, 2018.

Biermann, T., Babel, W., Ma, W., Chen, X., Thiem, E., Ma, Y., Foken, T.: Turbulent flux observations and modelling over a shallow lake and a wet grassland in the Nam Co basin, Tibetan Plateau, Theor. Appl. Climatol., 116(1–2), 301–316, https://doi. org/10.1007/s00704-013-0953-6, 2014.

Blyth, E., and Harding, R. J.: Methods to separate observed global evapotranspiration into the interception, transpiration and soil surface evaporation components, Hydrol. Process., 25(26), 4063–4068, https://doi.org/10.1002/hyp.8409, 2011.

Chang, Y., Qin, D., Ding, Y., Zhao, Q., Zhang, S: A modified MOD16 algorithm to estimate evapotranspiration over alpine meadow on the Tibetan Plateau, China, J. Hydrol., 561: 16–30, https://doi.org/10.1016/j.jhydrol.2018.03.054, 2018.

Chen, D., Xu, B., Yao, T., Guo, Z., Cui, P., Chen, F., Zhang, R., Zhang, X., Zhang, Y., Fan, J., Hou, Z., Zhang, T.: Assessment of past, present and future environmental changes on the Tibetan Plateau, Kexue Tongbao/Chinese Science Bulletin, 60(32), 3025–3035, https://doi.org/10.1360/N972014-01370, 2015.

Chen, X., Massman, W. J., Su, Z.: A Column Canopy-Air Turbulent Diffusion Method for Different Canopy Structures, J. Geophys. Res. Atmos., 124(2), 488–506, https://doi.org/10.1029/2018JD028883, 2019.

Chen, X., Su, Z., Ma, Y., Liu, S., Yu, Q., Xu, Z.: Development of a 10-year (2001–2010) 0.1° data set of land-surface energy balance for mainland China, Atmos. Chem. Phys., 14(23), 13097–13117, https://doi.org/10.5194/acp-14-13097-2014, 2014.

Chen, X., Su, Z., Ma, Y., Yang, K., Wen, J., Zhang, Y.: An Improvement of Roughness Height Parameterization of the Surface Energy Balance System (SEBS) over the Tibetan Plateau, J. Appl. Meteorol. Climatol., 52(3), 607–622, https://doi.org/10.1175/JAMC-D-12-056.1, 2013.

Chen, X., Su, Z., Ma, Y., Trigo, I., Gentine, P.: Remote Sensing of Global Daily Evapotranspiration based on a Surface

Energy Balance Method and Reanalysis Data, J. Geophys. Res. Atmos., 126(16), e2020JD032873, https://doi.org/10.1029/2020JD032873, 2021.

Chen, Y., Xia, J., Liang, S., Feng, J., Fisher, J. B., Li, X., Li, X., Liu, S., Ma, Z., Miyata, A., Mu, Q., Sun, L., Tang, J., Wang, K., Wen, J., Xue, Y., Yu, G., Zha, T., Zhang, L., Zhang, Q., Zhao, T., Zhao, L., Yuan, W.: Comparison of satellite-based evapotranspiration models over terrestrial ecosystems in China, Remote Sens. Environ., 140, 279–293, https://doi.org/10.1016/j.rse.2013.08.045, 2014.

Chen, Y., Yang, K., Tang, W., Qin, J., and Zhao, L.: Parameterizing soil organic carbon's impacts on soil porosity and thermal parameters for Eastern Tibet grasslands, Sci. China Earth Sci., 55(6), 1001–1011, https://doi.org/10.1007/s11430-012-4433-0, 2012.

Che, T., Li, X., Liu, S., Li, H., Xu, Z., Tan, J., Zhang, Y., Ren, Z., Xiao, L., Deng, J., Jin, R., Ma, M., Wang, J., and Yang, X.: Integrated hydrometeorological, snow and frozen-ground observations in the alpine region of the Heihe River Basin, China, Earth Syst. Sci. Data., 11, 1483–1499, https://doi.org/10.5194/essd-11-1483-2019, 2019.

Cleugh, H. A., Leuning, R., Mu, Q., Running, S. W.: Regional evaporation estimates from flux tower and MODIS satellite data, Remote Sens. Environ., 106(3), 285–304, https://doi.org/10.1016/j.rse.2006.07.007, 2007.

Cosby, B. J., Hornberger, G. M., Clapp, R. B., and Ginn, T. R.: A Statistical Exploration of the Relationships of Soil Moisture Characteristics to the Physical Properties of Soils, Water Resour. Res., 20(6), 682–690, https://doi.org/10.1029/WR020i006p00682, 1984.

Dan, J., Gao, Y., and Zhang, M.: tecting and Attributing Evapotranspiration Deviations Using Dynamical Downscaling and Convection-Permitting Modeling over the Tibetan Plateau, Water., 13(15), 2096: https://doi.org/10.3390/w13152096, 2017.

De Kok, R.J., Kraaijenbrink, P.D.A., Tuinenburg, O.A., Bonekamp, P.N.J., Immerzeel, W.W.: Towards understanding the pattern of glacier mass balances in High Mountain Asia using regional climatic modelling, Cryosphere, 14, 3215–3234, https://doi.org/10.5194/tc-14-3215-2020, 2020.

Denef, K., Galdo, I. D., Venturi, A., and Cotrufo, M. F.: Assessment of Soil C and N Stocks and Fractions across 11 European Soils under Varying Land Uses, Open J. Soil Sci., 03(07), 297–313, https://doi.org/10.4236/ojss.2013.37035, 2013.

Dore, S., Montes-Helu, M., Hart, S. C., Hungate, B. A., Koch, G. W., Moon, J. B., Finkral, A., Kolb, T. E.: Recovery of ponderosa pine ecosystem carbon and water fluxes from thinning and stand-replacing fire, Glob. Chang. Biol., 18(10), 3171–3185, https://doi.org/10.1111/j.1365-2486.2012.02775.x, 2012.

https://doi.org/10.5194/essd-2022-195
Preprint. Discussion started: 3 August 2022

Ding, J., Chen, L., Ji, C., Hugelius, G., Li, Y., Liu, L., Qin, S., Zhang, B., Yang, G., Li, F., Fang, K., Chen, Y., Peng, Y., Zhao, X., He, H., Smith, P., Fang, J., Yang, Y.: Decadal soil carbon accumulation across Tibetan permafrost regions, Nature Geoscience, 10(6), 420–424, https://doi.org/10.1038/ngeo2945, 2017.

Eyring, V., Bony, S., Meehl, G. A., Senior, C. A., Stevens, B., Stouffer, R. J., Taylor, K. E.: Overview of the Coupled Model Intercomparison Project Phase 6 (CMIP6) experimental design and organization, Geosci. Model Dev., 9, 1937–1958. https://doi.org/10.5194/gmd-9-1937-2016, 2016.

Farouki, O.T.: The thermal properties of soils in cold regions, Cold Reg. Sci., Technol. 5, 67–75, https://doi.org/10.1016/0165-232X(81)90041-0, 1981.

Fischer, M. L., Billesbach, D. P., Berry, J. A., Riley, W. J., and Torn, M. S.: Spatiotemporal variations in growing season exchanges of CO2, H2O, and sensible heat in agricultural fields of the Southern Great Plains, Earth Interact., 11(17), https://doi.org/10.1175/EI231.1, 2007.

Camillo, P. J. and Gurney, R. J.: A resistance parameter for bare soil evaporation models, Soil Sci., 141(2), 95–105, https://doi.org/10.1097/00010694-198602000-00001, 1986.

Gan, R., Zhang, Y., Shi, H., Yang, Y., Eamus, D., Cheng, L., Chiew, F., Yu, Q.: Use of satellite leaf area index estimating evapotranspiration and gross assimilation for Australian ecosystems, Ecohydrology, 11(5), e1974, https://doi.org/10.1002/eco.1974, 2018.

Good, S. P., Noone, D., and Bowen, G.: Hydrologic connectivity constrains partitioning of global terrestrial water fluxes, Science, 349(6244), 175–177, https://doi.org/10.1126/science.aaa5931, 2015.

Han, C., Ma, Y., Chen, X., Su, Z.: Trends of land surface heat fluxes on the Tibetan Plateau from 2001 to 2012, Int. J. Climatol., 37, 4757–4767, https://doi.org/10.1002/joc.5119, 2017.

Han, C., Ma, Y., Wang, B., Zhong, L., Ma, W., Chen, X., and Su, Z.: Long term variations of actual evapotranspiration over the Tibetan Plateau, Earth Syst. Sci. Data., 13, 3513–3524, https://doi.org/10.5194/essd-13-3513-202, 2021.

He, J., Yang, K., Tang, W., Lu, H., Qin, J., Chen, Y., Li, X.: The first high-resolution meteorological forcing dataset for land process studies over China, Sci. Data., 7(1), 25, https://doi.org/10.1038/s41597-020-0369-y, 2020.

Immerzeel, W. W., Lutz, A. F., Andrade, M., Bahl, A., Biemans, H., Bolch, T., Hyde, S., Brumby, S., Davies, B., Elmore, A., Emmer, A., Feng, M., Fernández, A., Haritashya, U., Kargel, J., Koppes, M., Kraaijenbrink, P., Kulkarni, A., Mayewski, P., Nepal, S., Pacheco, P., Painter, T., Pellicciotti, F., Rajaram, H., Rupper, S., Sinisalo, A., Shrestha, A., Viviroli, D., Wada, Y., Xiao, C., Yao, T., Baillie, J. E. M.: Importance and vulnerability of the world's water towers, Nature, 577(7790), 364–369, https://doi.org/10.1038/s41586-019-

1822-y, 2020.

Irmak, S., and Mutiibwa, D.: On the dynamics of canopy resistance: Generalized linear estimation and relationships with primary micrometeorological variables, Water Resour. Res., 46(8), W08526, https://doi.org/10.1029/2009WR008484, 2010.

Jarvis, P. G.: The InterprETtion of the Variations in Leaf Water Potential and Stomatal Conductance Found in Canopies in the Field. Philos, Trans. R. Soc. London. B, Biol. Sci., 273(927), 593–610, https://doi.org/10.1098/rstb.1976.0035, 1976.

Jung, M., Reichstein, M., Ciais, P., Seneviratne, S. I., Sheffield, J., Goulden, M. L., Bonan, G., Cescatti, A., Chen, J., De Jeu, R., Dolman, A., Eugster, W., Gerten, D., Gianelle, D., Gobron, N., Heinke, J., Kimball, J., Law, B., Montagnani, L., Mu, Q., Mueller, B., Oleson, K., Papale, D., Richardson, A., Roupsard, O., Running, S., Tomelleri, E., Viovy, N., Weber, U., Williams. C., Wood, E., Zaehle, S., Zhang, K.: Recent decline in the global land evapotranspiration trend due to limited moisture supply, Nature, 467(7318), 951–954, https://doi.org/10.1038/nature09396, 2010.

Khan, M. S., Liaqat, U. W., Baik, J., and Choi, M.: Stand-alone uncertainty characterization of GLEAM, GLDAS and MOD16 evapotranspiration products using an extended triple collocation approach, Agric. For. Meteorol., 252, 256–268, https://doi.org/10.1016/j.agrformet.2018.01.022, 2018.

Kuang, X., and Jiao, J. J.: Review on climate change on the Tibetan plateau during the last half century, J. Geophys. Res. Atmos., 121, 3979-4007, https://doi.org/10.1002/2015JD024728, 2016.

Kutsch, W. L., Aubinet, M., Buchmann, N., Smith, P., Osborne, B., Eugster, W., Wattenbach, M., Schrumpf, M., Schulze, E., Tomelleri, E., Ceschia, E., Bernhofer, C., Béziat, P., Carrara, A., Di Tommasi, P., Grunwald, T., Jones, M., Magliulo, V., Moureaux, C., Olioso, A., Sanz, M., Saunders, M., Sǿgaard, H., Ziegler, W.: The net biome production of full crop rotations in Europe, Agric. Ecosyst. Environ., 139(3), 336–345, https://doi.org/10.1016/j.agee.2010.07.016, 2010.

Kool, D., Agam, N., Lazarovitch, N., Heitman, J.L., Sauer, T.J., Ben-Gal, A.: A review of approaches for evapotranspiration partitioning, Agric. For. Meteorol., 184, 56–70, https://doi.org/10.1016/j.agrformet.2013.09.003, 2014.

Koster, R. D., and Suarez, M. J.: The Influence of Land Surface Moisture Retention on Precipitation Statistics. J. Clim., 9(10), 2551–2567, https://doi.org/10.1175/1520-0442(1996)009, 1996.

Lawrence, D. M., Thornton, P. E., Oleson, K. W., and Bonan, G. B.: The Partitioning of Evapotranspiration into Transpiration, Soil Evaporation, and Canopy Evaporation in a GCM: Impacts on Land–Atmosphere

Interaction, J. Hydrometeorol., 8, 862–880, https://doi.org/10.1175/JHM596.1, 2007.

Lehmann, P., Merlin, O., Gentine, P., and Or, D.: Soil texture effects on surface resistance to bare soil evaporation, Geophys. Res. Lett., 45(19), 10, 398-10, 405, https://doi.org/10.1029/2018GL078803, 2018.

Lemone, M. A., Chen, F., Alfieri, J. G., Cuenca, R. H., Hagimoto, Y., Blanken, P., Niyogi, D., Kang, S., Davis, K., Grossman, R. L.: NCAR/CU surface, soil, and vegetation observations during the International H2O Project 2002 field campaign, Bull. Am. Meteorol. Soc, 88(1), 65–81, https://doi.org/10.1175/BAMS-88-1-65, 2007.

Letts, M.G., Comer, N.T., Roulet, N.T., Skarupa, M.R., Verseghy, D.L.: Parametrization of peatland hydraulic properties for the Canadian land surface scheme, Atmos. Ocean., 38, 141–160, https://doi.org/10.1080/07055900.2000.9649643, 2000.

Leuning, R., Zhang, Y.Q., Rajaud, A., Cleugh, H., Tu, K.: A simple surface conductance model to estimate regional evaporation using MODIS leaf area index and the Penman–Monteith equation, Water Resour., Res. 44 (10), W10419, https://doi.org/10.1029/2007WR006562, 2010.

Liang, S., Cheng, J., Jia, K., Jiang, B., Liu, Q., Xiao, Z., Yao, Y., Yuan, W., Zhang, X., Zhao, X., Zhou, J.: The global land surface satellite (GLASS) product suite, Bull. Am. Meteorol. Soc., 102, E323–E337, https://doi.org/10.1175/BAMS-D-18-0341.1, 2021.

Liu, J., Chai, L., Dong, J., Zheng, D., Wigneron, J. P., Liu, S., Zhou, J., Xu, T., Yang, S., Song, Y., Qu, Y., Lu, Z.: Uncertainty analysis of eleven multisource soil moisture products in the third pole environment based on the three-corned hat method, Remote Sens. Environ., 255, 112225, https://doi.org/10.1016/j.rse.2020.112225, 2021.

Liu, S.M., Li, X., Xu, Z.W., Che, T., Xiao, Q., Ma, M.G., Liu, Q.H., Jin, R., Guo, J.W., Wang, L.X., Wang, W.Z., Qi, Y., Li, H.Y., Xu, T.R., Ran, Y.H., Hu, X.L., Shi, S.J., Zhu, Z.L., Tan, J.L., Zhang, Y., Ren, Z.G.: The Heihe Integrated Observatory Network: A Basin-Scale Land Surface Processes Observatory in China, Vadose Zo. J., 17(1), 180072, https://doi.org/10.2136/vzj2018.04.0072, 2018.

Liu, S. M., Xu, Z. W., Wang, W. Z., Jia, Z. Z., Zhu, M. J., Bai, J., and Wang, J. M.: A comparison of eddy-covariance and large aperture scintillometer measurements with respect to the energy balance closure problem, Hydrol. Earth Syst. Sci., 15, 1291–1306, https://doi.org/10.5194/hess-15-1291-2011, 2011.

Li, S., Hao, X., Du, T., Tong, L., Zhang, J., Kang, S.: A coupled surface resistance model to estimate crop evapotranspiration in arid region of northwest China, Hydrol. Process., 28(4), 2312–2323, https://doi.org/10.2136/vzj2018.04.0072, 2013.

Li, S., Wang, G., Sun, S., Chen, H., Bai, P., Zhou, S., Huang, Y., Wang, J., Deng, P.: Assessment of Multi-Source

Evapotranspiration Products over China Using Eddy Covariance Observations, Remote Sens., 10(11), 1692, https://doi.org/10.3390/rs10111692, 2018.

Li, X., Liang, S., Yuan, W., Yu, G., Cheng, X., Chen, Y., Zhao, T., Feng, J., Ma, Z., Ma, M., Liu, S., Chen, J., Shao, C., Li, S., Zhang, X., Zhang, Z., Sun, G., Chen, S., Ohta, T., Varlagin, A., Miyata, A., Takagi, K., Saiqusa, N., Kato, T.: Estimation of evapotranspiration over the terrestrial ecosystems in China, Ecohydrology, 7(1), 139–149, https://doi.org/10.1002/eco.1341, 2014a.

Li, X., Wang, L., Chen, D., Yang, K., and Wang, A.: Seasonal evapotranspiration changes (1983-2006) of four large basins on the Tibetan Plateau, J. Geophys. Res. Atmos., 119(23), 13,079–13,095, https://doi.org/10.1002/2014JD022380, 2014b.

Li, S., Zhang, L., Kang, S., Tong, L., Du, T., Hao, X., and Zhao, P.: Comparison of several surface resistance models for estimating crop evapotranspiration over the entire growing season in arid regions, Agric. For. Meteorol., 208, 1–15, https://doi.org/10.1016/j.agrformet.2015.04.002, 2015.

Long, D., Singh, V. P., and Li, Z.-L.: How sensitive is SEBAL to changes in input variables, domain size and satellite sensor?, J. Geophys. Res.-Atmos., 116, D21107, https://doi.org/10.1029/2011jd016542, 2011.

Ma, N., Szilagyi, J., Zhang, Y., Liu, W.: Complementary-Relationship-Based Modeling of Terrestrial Evapotranspiration Across China During 1982–2012: Validations and Spatiotemporal Analyses, J. Geophys. Res. Atmos., 124(8), 4326–4351, https://doi.org/10.1029/2018JD029850, 2019.

Ma, N., Zhang, Y.: Increasing Tibetan Plateau terrestrial evapotranspiration primarily driven by precipitation, Agric. For. Meteorol., 317, 108887, https://doi.org/10.1016/j.agrformet.2022.108887, 2022.

Ma, N., Zhang, Y., Guo, Y., Gao, H., Zhang, H., Wang, Y.: Environmental and biophysical controls on the evapotranspiration over the highest alpine steppe, J. Hydrol., 529, 980–992, https://doi.org/10.1016/j.jhydrol.2015.09.013, 2015.

Ma, Y., Hu, Z., Xie, Z., Ma, W., Wang, B., Chen, X., Li, M., Zhong, L., Sun, F., Gu, L., Han, C., Zhang, L., Liu, X., Ding, Z., Sun, G., Wang, S., Wang, Y., and Wang, Z.: A long-term (2005–2016) dataset of hourly integrated land–atmosphere interaction observations on the Tibetan Plateau, Earth Syst. Sci. Data., 12, 2937–2957, https://doi.org/10.5194/essd-12-2937-2020, 2020.

Merlin, O., Stefan, V. G., Amazirh, A., Chanzy, A., Ceschia, E., Er-Raki, S., Khabba, S.: Modeling soil evaporation efficiency in a range of soil and atmospheric conditions using a meta-analysis approach, Water Resour. Res., 52(5), 3663–3684, https://doi.org/10.1002/2015WR018233, 2016.

Miralles, D. G., Holmes, T. R. H., De Jeu, R. A. M., Gash, J. H., Meesters, A. G. C. A., Dolman, A. J.: Global land-surface evaporation estimated from satellite-based observations, Hydrol. Earth Syst. Sci., 15(2), 453–469, https://doi.org/10.5194/hess-15-453-2011, 2011.

Miralles, D. G., Jiménez, C., Jung, M., Michel, D., Ershadi, A., McCabe, M. F., Hirschi, M., Martens, B., Dolman, A. J., Fisher, J. B., Mu, Q., Seneviratne, S. I., Wood, E. F., and Fernández-Prieto, D.: The WACMOS-ET project – Part 2: Evaluation of global terrestrial evaporation data sets, Hydrol. Earth Syst. Sci., 20, 823–842, https://doi.org/10.5194/hess-20-823-2016, 2016.

Monteith, J.L.: Evaporation and environment. Symp. Soc. Exp. Biol., 19, 205–234, 1965.

Muñoz-Sabater, J., Dutra, E., Agustí-Panareda, A., Albergel, C., Arduini, G., Balsamo, G., Boussetta, S., Choulga, M., Harrigan, S., Hersbach, H., Martens, B., Miralles, D., Piles, M., Rodríguez-Fernández, N., Zsoter, E., Thépaut, J. N.: ERA5-Land: A state-of-the-art global reanalysis dataset for land applications, Earth Syst. Sci. Data, 13(9), 4349–4383, https://doi.org/10.5194/essd-13-4349-2021, 2021.

Mu, Q., Heinsch, F. A., Zhao, M., and Running, S. W.: Development of a global evapotranspiration algorithm based on MODIS and global meteorology data, Remote Sens. Environ., 111(4), 519–536. https://doi.org/10.1016/j.rse.2007.04.015, 2007.

Mu, Q., Zhao, M., and Running, S. W.: Improvements to a MODIS global terrestrial evapotranspiration algorithm, Remote Sens. Environ., 115(8), 1781–1800, https://doi.org/10.1016/j.rse.2011.02.019, 2011.

Novick, K. A., Stoy, P. C., Katul, G. G., Ellsworth, D. S., Siqueira, M. B. S., Juang, J., Oren, R.: Carbon dioxide and water vapor exchange in a warm temperate grassland, Oecologia., 138(2), 259–274, https://doi.org/10.1007/s00442-003-1388-z, 2004.

Ortega-Farias, S., Poblete-Echeverría, C., and Brisson, N.: Parameterization of a two-layer model for estimating vineyard evapotranspiration using meteorological measurements, Agric. For. Meteorol., 150(2), 276–286, https://doi.org/10.1016/j.agrformet.2009.11.012, 2010.

Peng, J., Loew, A., Chen, X., Ma, Y., and Su, Z.: Comparison of satellite-based evapotranspiration estimates over the Tibetan Plateau. Hydrol, Earth Syst. Sci., 20, 3167–3182, https://doi.org/10.5194/hess-20-3167-2016, 2016.

Phillips, T. J., Klein, S. A., Ma, H. Y., Tang, Q., Xie, S., Williams, I. N., Joseph, A., David, R., Margaret, S.: Using ARM observations to evaluate climate model simulations of land-atmosphere coupling on the U.S. Southern Great Plains, J. Geophys. Res. Atmos., 122(21), 11,524–11, 548, https://doi.org/10.1002/2017JD027141, 2017.

Ramoelo, A., Majozi, N., Mathieu, R., Jovanovic, N., Nickless, A., and Dzikiti, S.: Validation of Global Evapotranspiration Product (MOD16) using Flux Tower Data in the African Savanna, South Africa, Remote

https://doi.org/10.5194/essd-2022-195
Preprint. Discussion started: 3 August 2022

Sens.-Basel, 6, 7406–7423, https://doi.org/10.3390/rs6087406, 2014.

Rodell, M., Houser, P. R., Jambor, U., Gottschalck, J., Mitchell, K., Meng, C. J., Arsenault, K., Cosgrovem B., Radakovich, J., Bosilovich, M., Entin, J., Walker, J., Lohmann, D., Toll, D.: The Global Land Data Assimilation System, Bull. Am. Meteorol. Soc., 85, 381–394, https://doi.org/10.1175/BAMS-85-3-381, 2004.

Sakaguchi, K., Zeng, X.: Effects of soil wetness, plant litter, and under-canopy atmospheric stability on ground evaporation in the Community Land Model (CLM3.5), J. Geophys. Res., Atmos. 114(D1), https://doi.org/10.1029/2008JD010834, 2009.

Sellers, P. J., Randall, D. A., Collatz, G. J., Berry, J. A., Field, C. B., Dazlich, D. A., and Bounoua, L.: A Revised Land Surface Parameterization (SiB2) for Atmospheric GCMS. Part I: Model Formulation, J. Clim. 9(4), 676–705, https://doi.org/10.1175/1520-0442(1996)009<0676:ARLSPF>2.0.CO;2, 1996.

Schlesinger, W. H., and Jasechko, S.: Transpiration in the global water cycle, Agric. For. Meteorol., 189-190, 115–117, https://doi.org/10.1016/j.agrformet.2014.01.011, 2014.

Shi, Q., Liang, S.:Surface-sensible and latent heat fluxes over the Tibetan Plateau from ground measurements, reanalysis, and satellite data, Amos. Chem. Phys.,14, 5659–5677, https://doi.org/10.5194/acp-14-5659-2014, 2014.

Sobrino, J. A., Jiménez-Muñoz, J. C., and Paolini, L.: Land surface temperature retrieval from LANDSAT TM 5, Remote Sens. Environ., 90(4), 434–440, https://doi.org/10.1016/j.rse.2004.02.003, 2004.

Song, L., Zhuang, Q., Yin, Y., Zhu, X., and Wu, S.: Spatio-temporal dynamics of evapotranspiration on the Tibetan Plateau from 2000 to 2010, Environ. Res. Lett., 12(1), 014011, https://doi.org/10.1088/1748-9326/aa527d, 2017.

Su, Z.: The Surface Energy Balance System (SEBS) for estimation of turbulent heat fluxes, Hydrol. Earth Syst. Sci., 6, 85–100, https://doi.org/10.5194/hess-6-85-2002, 2002.

Sun, S.F.: Moisture and heat transport in a soil layer forced by atmospheric conditions, Master thesis, Dept. of Civil Engineering, University of Connecticut, 72, 1982.

Tang, J. Y. and Riley, W. J.: A new top boundary condition for modeling surface diffusive exchange of a generic volatile tracer: theoretical analysis and application to soil evaporation, Hydrol. Earth Syst. Sci., 17, 873–893, https://doi.org/10.5194/hess-17-873-2013, 2013.

Wang, B., Ma, Y., Su, Z., Wang, Y., and Ma, W.: Quantifying the evaporation amounts of 75 high-elevation large dimictic lakes on the Tibetan Plateau, Sci. Adv., 6(26), https://doi.org/10.1126/sciadv.aay8558, 2020.

Wang, G., Lin, S., Hu, Z., Lu, Y., Sun, X., and Huang, K.: Improving Actual Evapotranspiration Estimation

Integrating Energy Consumption for Ice Phase Change Across the Tibetan Plateau, J. Geophys. Res. Atmos., 125(3), e2019JD031799, https://doi.org/10.1029/2019JD031799, 2020.

Wang, W., Li, J., Yu, Z., Ding, Y., Xing, W., Lu, W.: Satellite retrieval of actual evapotranspiration in the Tibetan Plateau: components partitioning, multi decadal trends and dominated factors identifying, J. Hydrol., 559, 471–485, https://doi.org/10.1016/j.jhydrol.2018.02.065, 2018.

Wieder, W.R., J. Boehnert, G.B. Bonan, and M. Langseth.: Regridded Harmonized World Soil Database v1.2. Data set, Available on-line [http://daac.ornl.gov] from Oak Ridge National Laboratory Distributed Active Archive Center, Oak Ridge, Tennessee, USA, http://dx.doi.org/10.3334/ORNLDAAC/1247, 2014.

Wilcox, B.P., Breshears, D.D., Seyfried, M.S.: Water balance on rangelands, In: Stewart, B.A., Howell, T.A. (Eds.), Encyclopedia of Water Science, Marcel Dekker Inc, New York, 791–794, http://www.cprl.ars.usda.gov/wmru/pdfs/DekkerEvettTDR.pdf, 2003.

Wu, C., Hu, B. X., Huang, G., and Zhang, H.: Effects of climate and terrestrial storage on temporal variability of actual evapotranspiration, J. Hydrol., 549, 388–403, https://doi.org/10.1016/j.jhydrol.2017.04.012, 2017.

Xie, H., Zhu, X., Yuan, D.Y.: Pan evaporation modelling and changing attribution analysis on the Tibetan Plateau (1970-2012), Hydrol. Process., 29, 2164-2177, https://doi.org/10.1002/hyp.10356, 2015.

Yang, K., He, J., Tang, W., Qin, J., Cheng, C. C. K.: On downward shortwave and longwave radiations over high altitude regions: Observation and modeling in the Tibetan Plateau, Agric. For. Meteorol., 150(1), 38–46, https://doi.org/10.1016/j.agrformet.2009.08.004, 2010.

Yang, K., Koike, T., Ishikawa, H., Kim, J., Li, X., Liu, H., Liu S., Ma Y., Wang, J.: Turbulent flux transfer over bare-soil surfaces: Characteristics and parameterization, J. Appl. Meteorol. Climatol., 47(1), 276–290, https://doi.org/10.1175/2007JAMC1547.1, 2008.

Yang, K., Wu, H., Qin, J., Lin, C., Tang, W., and Chen, Y.: Recent climate changes over the Tibetan Plateau and their impacts on energy and water cycle: A review, Glob. Planet. Change., 112, 79–91, https://doi.org/10.1016/j.gloplacha.2013.12.001, 2014.

Yang, Y., Liu, Y., Li, M., Hu, Z., Ding, Z.: Assessment of reanalysis flux products based on eddy covariance observations over the Tibetan Plateau, Theor. Appl. Climatol., 138, 275–292, https://doi.org/10.1007/s00704-019-02811-1, 2019.

Yao, T., Lu, H., Feng, W., Yu, Q.: Evaporation abrupt changes in the Qinghai-Tibet Plateau during the last half-century, Sci. Rep., 9(1), 20181, https://doi.org/10.1038/s41598-019-56464-1, 2019.

Yao, T., Thompson, L., Yang, W., Yu, W., Gao, Y., Guo, X., Yang, X., Duan, K., Zhao, H., Xu, B., Pu, J., Lu, A., Xiang, Y., Kattel, D., Joswiak, D.: Different glacier status with atmospheric circulations in Tibetan Plateau and surroundings, Nature Clim. Change, 2(9), 663–667, https://doi.org/10.1038/nclimate1580, 2012.

Yao, Y., Liang, S., Cheng, J., Liu, S., Fisher, J. B., Zhang, X., Jia, K., Zhao, X., Qin, Q., Zhao, B., Han, S., Zhou, G., Li, Y., Zhao, S.: MODIS-driven estimation of terrestrial latent heat flux in China based on a modified Priestley-Taylor algorithm, Agric. For. Meteorol., 171–172, 187–202, https://doi.org/10.1016/j.agrformet.2012.11.016, 2013.

Yin, Y., Wu, S., Zhao, D., Zheng, D., Pan, T.: Modeled effects of climate change on actual evapotranspiration in different eco-geographical regions in the Tibetan Plateau, J. Geogr. Sci., 23(2), 195–207, https://doi.org/10.1002/eco.1341, 2013.

You, Q., Xue, X., Peng, F., Dong, S., Gao, Y.: Surface water and heat exchange comparison between alpine meadow and bare land in a permafrost region of the Tibetan Plateau, Agric. For. Meteorol., 232, 48–65, https://doi.org/10.1016/j.agrformet.2016.08.004, 2017.

Yuan, L., Ma, Y., Chen, X., Wang, Y., Li, Z.: An enhanced MOD16 evapotranspiration model for the Tibetan Plateau during the unfrozen season, J. Geophys. Res. Atmos., 126, e2020JD032787, https://doi.org/10.1029/2020JD032787, 2021.

Yu, G. R., Wen, X. F., Sun, X. M., Tanner, B. D., Lee, X., Chen, J. Y.: Overview of ChinaFLUX and evaluation of its eddy covariance measurement, Agric. For. Meteorol., 137(3–4), 125–137, https://doi.org/10.1016/j.agrformet.2006.02.011, 2006.

Zhang, C., Liu, F., and Shen, Y.: Attribution analysis of changing pan evaporation in the Qinghai–Tibetan Plateau, China, Int. J. Climatol., 38, e1032–e1043, https://doi.org/10.1002/joc.5431, 2018.

Zhang, L. M., Luo, Y. W., Liu, M., Chen, Z., Su, W., He et al.: Carbon and water fluxes observed by the Chinese Flux Observation and Research Network (2003–2005) (in Chinese), Sci. Data., 4(1), https://doi.org/10.11922/csdata.2018.0028.zh, 2019.

Zhang, K., Kimball, J. S., Nemani, R. R., and Running, S. W.: A continuous satellite-derived global record of land surface evapotranspiration from 1983 to 2006, Water Resour. Res., 46(9), W09522, https://doi.org/10.1029/2009WR008800, 2010.

Zhang, Y., Kong, D., Gan, R., Chiew, F. H. S., McVicar, T. R., Zhang, Q., and Yang, Y.: Coupled estimation of 500 m and 8-day resolution global evapotranspiration and gross primary production in 2002–2017, Remote Sens. Environ., 222, 165–182, https://doi.org/10.1016/j.rse.2018.12.031, 2019b.

Zhang, Y., Peña-Arancibia, J. L., McVicar, T. R., Chiew, F. H. S., Vaze, J., Liu, C., Lu, X., Zheng, H., Wang, Y., Liu,

https://doi.org/10.5194/essd-2022-195
Preprint. Discussion started: 3 August 2022

Open Access Earth System Science Data Discussions

Y., Miralles, D., Pan, M.: Multi-decadal trends in global terrestrial evapotranspiration and its components, Sci. Rep., 6, 19124, https://doi.org/10.1038/srep19124, 2016.

Zhao, H., Zeng, Y., Lv, S., and Su, Z.: Analysis of soil hydraulic and thermal properties for land surface modeling over the Tibetan Plateau, Earth Syst. Sci. Data., 10, 1031–1061, https://doi.org/10.5194/essd-10-1031-2018, 2018.

Zheng, D., Zhang, Q., Wu, S.: Mountain geoecology and sustainable development of the Tibetan Plateau, Springer Science & Business Media, 57, 2000.

Zhong, L., Ma, Y., Hu, Z., Fu, Y., Hu, Y., Wang, X., Cheng, M., and Ge, N.: Estimation of hourly land surface heat fluxes over the Tibetan Plateau by the combined use of geostationary and polar-orbiting satellites, Atmos. Chem. Phys., 19, 5529–5541, https://doi.org/10.5194/acp-19-5529-2019, 2019.

Zohaib, M., H. Kim, and M. Choi.: Evaluating the patterns of spatiotemporal trends of root zone soil moisture in major climate regions in East Asia, J. Geophys. Res. Atmos., 122, 7705–7722, https://doi.org/10.1002/2016JD026379, 2017.